

# INTERFEROMETRY AND APERTURE SYNTHESIS

*Edward B. Fomalont and Melvyn C. H. Wright*

## 10.1 Basic Concepts

### 10.1.1 The Need for High Resolution in a Telescope

The resolution of a telescope has a diffraction limit of  $\sim \lambda/D$ , where  $\lambda$  is the observing wavelength and  $D$  is the aperture diameter. The resolution of large optical telescopes is limited to about a half arc second by atmospheric fluctuations, although the diffraction limit is much smaller. However, for radio frequencies a diffraction limit of about 1 arc minute at the highest radio frequencies is currently reached using filled-aperture telescopes. Further significant increase of the resolution of filled-aperture telescopes is not likely.

Many sources of radio radiation are confined to small angular extents, and a resolution much higher is needed to help understand the physical processes in radio sources. The majority of extra-galactic radio sources are smaller than 1 arc minute and some radio components have not yet been resolved ( $< 3 \times 10^{-4}$  arc second) using intercontinental baselines. Radio emission in our galaxy, though resolved with filled-aperture telescopes, nevertheless shows fine-scale structure in the second of arc range. The study of spectral-line radiation associated with molecules in space also requires high-resolution studies. Some maser emission regions are extremely small, and some of the

larger clouds of molecular emission show small spatial clumps in their associated emission and absorption profiles. The mapping of hydrogen using the 21-cm transition frequency is limited to the very nearest galaxies with a filled-aperture telescope.

The sensitivity for observations of continuum radiation is often limited, not by receiver noise, but by confusion. There is little usefulness in increasing the sensitivity beyond the point where more than one source is likely to be within the antenna beam. The density of sources is such that to reach the confusion limit of a large antenna with the best receivers requires a few minutes or less of integration time. Better sensitivity can be fully utilized only in connection with increased resolution.

The need for high resolution was recognized with the first radio interferometers used in the late 1940's (Ryle and Vonberg, 1946; McCready *et al.*, 1947). The work of Stanier (1950) showed that an interferometer could be used to measure the Fourier components of a brightness distribution, and developments by Ryle and co-workers in England and by Christiansen and Mills and co-workers in Australia (Ryle, 1952; Christiansen, 1953; Mills and Little, 1953) extended interferometry to multi-elements and movable elements. The detailed principle of aperture synthesis was formulated by Ryle and Hewish (1960).

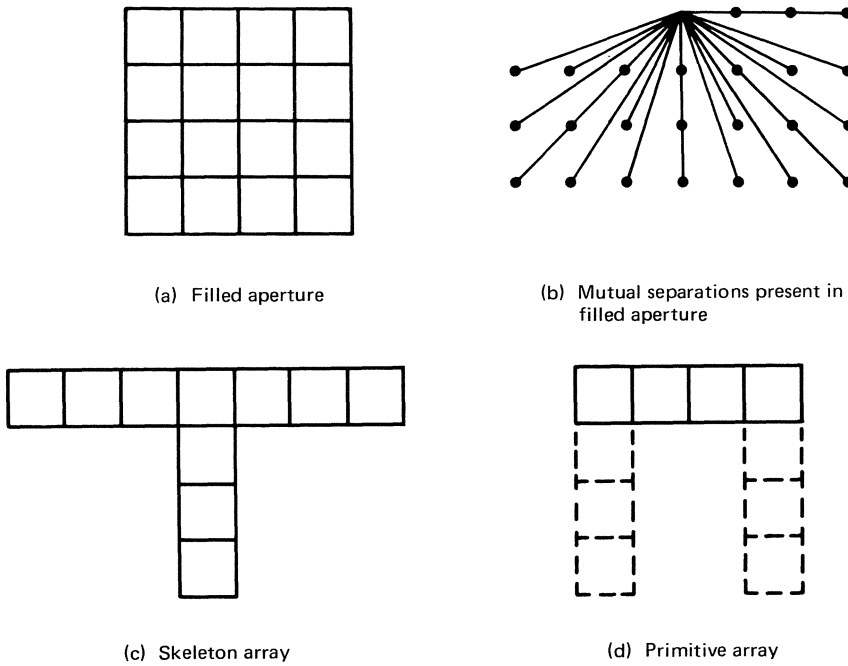


**Figure 10.1** Principle of aperture synthesis. (a) Filled aperture consisting of 16 elemental areas. (b) Vectors indicating the 24 separations present in the filled aperture. (c) A “Tee” skeleton array consisting of 10 elemental areas and spanning the same mutual separations as the filled aperture. (d) A primitive array consisting of four stationary elements and six locations for one or more additional moveable elements.

10.1.2 Aperture Synthesis Technique

There are many methods of obtaining high resolution, and all involve the placing of receiving elements, suitably connected, over a large area. The speed at which a large aperture is synthesized depends upon the arrangement, the number, and the mobility of the elements. In the study of radio sources whose emission is not time-variable, it is not necessary that the whole of the telescope aperture be present at the same time. Following Ryle and Hewish (1960), the principle behind aperture synthesis may be understood by considering the operation of a conventional, filled-aperture telescope, which may be regarded as composed of  $N$  elemental areas as in Figure 10.1(a). For convenience a square aperture with  $N = 16$  is taken. The signal in the  $n$ th area due to a source of emission is

$$I_n \cos(\omega t + \phi_n) \tag{10.1}$$

where  $I_n$  is the amplitude of the signal and  $\phi_n$  is the relative phase of the radiation. The relative phase over the aperture depends on the source direction. If the signals from the elements are added together vectorially (as, for example, by the feed at the focus of a parabolic reflector) and time-averaged, the power output is

$$\begin{aligned}
 P &\propto \frac{1}{2} \sum_{j=1}^N \sum_{k=1}^N I_j I_k \cos(\phi_j - \phi_k) \\
 &= \frac{1}{2} \sum_{j=1}^N I_j^2 + \sum_{j=1}^{N-1} \sum_{k=j+1}^N I_j I_k \cos(\phi_j - \phi_k)
 \end{aligned}
 \tag{10.2}$$

The first term is proportional to the sum of the powers received by the elementary areas. The resolving power, which is related to how  $P$  changes with the direction of the source (and hence with  $\phi_n$ ), derives from the cross-product terms. Each individual term can equally well be measured with just two ele-

mentary areas in positions  $j$  and  $k$ . All the terms can accordingly be measured sequentially with only two elementary areas which can be moved about on the ground. The summation of the cross products thus measured can be performed later, e.g., in a digital computer. This is the principle of aperture synthesis: The two elementary areas can be used to synthesize the result of a measurement with the much larger area (the “synthesized aperture”).

The term  $\phi_j - \phi_k$  can be written as  $(2\pi/\lambda) \mathbf{B}_{jk} \cdot \mathbf{s}$ , where  $\mathbf{B}_{jk}$  is the separation of the two elemental areas,  $\mathbf{s}$  is a unit vector defining the source position, and  $\lambda$  is the wavelength of the radiation.

Although there are  $N(N - 1)/2$  cross-product terms, many occur with redundancy. The aperture in Figure 10.1(a) with 120 cross-product terms has only 24 independent mutual separations, with highest redundancy occurring in the close separations. These basic separations are shown in Figure 10.1(b).

An array which contains all of the relative positions of a filled aperture is called a skeleton array. The “Tee” array in Figure 10.1(c) is an example. Only 10 elemental areas are needed to span the filled rectangular aperture. More generally, if we decompose a square aperture into an  $(n \times n)$  elemental area, the corresponding “Tee” skeleton array contains only  $3n - 2$  elemental areas. There are many examples of skeleton arrays; e.g., a ring-shaped configuration is a skeleton array for a filled circular aperture (Wild, 1967).

The redundancy of the mutual separations for a skeleton array is, however, different than that for an equivalent filled aperture. This leads to a different beam pattern and sidelobe level. Also, the discrete nature of the mutual separations in a skeleton array leads to grating sidelobes. These properties are discussed in more detail in section 10.3.

An aperture may be synthesized by physically moving elements on the ground to occupy in turn all relative positions that occur in the aperture. Thus even with a two-element interferometer, it is possible to span completely a large aperture. Such arrays are called primitive arrays. For example, as seen in

Figure 10.1(d), the array of four fixed elements and one moveable element is able to synthesize the desired aperture with six locations of the moveable element. Alternatively, with two moveable elements, only three configurations are necessary. The Cambridge 4C survey (Ryle, 1960) used a scheme where one arm of a “Tee” array was constructed and the other arm was obtained by moving a small element in a perpendicular direction. For these arrays the addition of the separate configurations are usually performed in a digital computer after the set of observation has been completed.

One method, developed at Cambridge (e.g., Ryle, 1962), uses the rotation of the Earth to change the aspect of the array. This method is illustrated in Figure 10.2. As viewed from the radio source, the array (assumed to be a two-element interferometer oriented in the east-west direction) rotates through all possible orientations over a period of 12 hours. With Earth rotation an aperture can be synthesized using a relatively small number of elements aligned in one direction. A line aperture is obtained instantaneously with the array, and this line

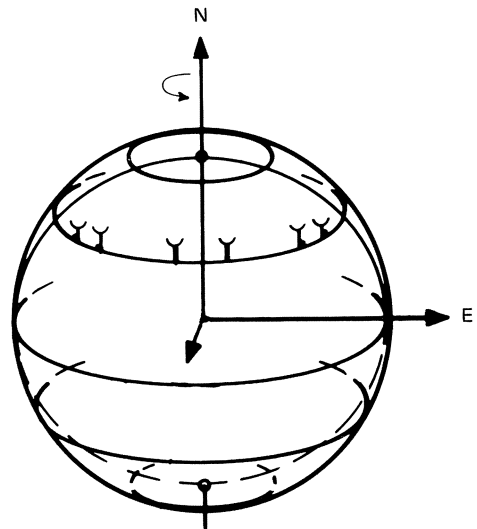


**Figure 10.2** The rotation and foreshortening of a two-element east-west interferometer due to the rotation of the Earth as seen by an observer at the source.

aperture is rotated by the Earth's rotation.

The redundancy of the separations for a primitive array, as with a skeleton array, is different from that of the equivalently filled aperture. However, when performing the summation in a digital computer, an advantage is that the different separations may be combined with any desired weighting. One can in this way compensate for the differences in redundancy and so make the resultant weighting correspond more closely to that of a filled aperture (see Section 10.3).

For the most part we will concentrate on primitive arrays which utilize the Earth's rotation. Most of the newer or planned arrays are of this type. Often the arrays are built with elements aligned in one or in several directions, with moveable telescopes to fill in spacings along an array axis or to change the resolution of the array.

The building block of all arrays, the two-element interferometer, is discussed in the remainder of Section 10.1. The geometry needed for Earth rotation synthesis, the measurement of the visibility function, effects of bandwidth, polarimetry, and a tabulation of useful formulae in the Appendix are discussed. In Section 10.2 a working interferometer is briefly discussed. Variations of the usual techniques are also covered. Aperture synthesis techniques and problems are reviewed in Section 10.3. Sensitivity problems are also discussed. Finally in Section 10.4 the inversion processes for obtaining maps of the source brightness from interferometric data are outlined.

### 10.1.3 Two-Element Interferometer

#### a) Response to a Point Source

The two-element interferometer provides high resolution by correlating the signals of the two antennas. The correlation is normally achieved by the multiplication or addition of the signals, which produces a spatial modulation of the primary beam of the antennas with interference fringes. In this way fine structure is introduced into the primary beam to increase the resolution.

The response of the system to a point source of monochromatic radiation of frequency  $\omega$  or wavelength  $\lambda$  is shown in Figure 10.3. A voltage  $E$  proportional to the electric field caused by the source is generated at the feed of each telescope at slightly different times. This time difference is called the geo-

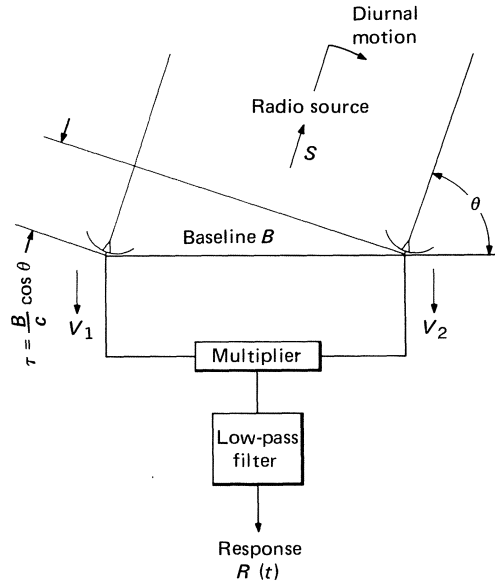


Figure 10.3 A simple two-element correlating interferometer.

metric delay and is denoted by  $\tau$ . The voltages at the multiplier input are

$$\begin{aligned} V_1 &\propto E \cos(\omega t) \\ V_2 &\propto E \cos[\omega(t - \tau)] \\ &= E \cos\left(\omega t - \frac{2\pi B}{\lambda} \cos \theta\right) \end{aligned} \quad (10.3)$$

where  $B$  is the separation of the two antennas,  $\lambda$  is the wavelength of the radiation, and  $\theta$  is the angle between the point source and the line joining the two antennas. The expression  $(B/\lambda) \cos \theta$ , the interference term, gives the phase path-length difference of the radiation travel along the two possible paths. The diurnal motion of the Earth causes  $\theta$  to vary with time. The output,  $R(t)$ , of the multiplier,

after a high-frequency term is rejected by a low pass filter, is

$$R(t) \propto S \cos \left( \frac{2\pi B}{\lambda} \cos \theta(t) \right) \quad (10.4)$$

This is the basic equation of interferometry. The flux density, or power  $S$ , of the source has replaced  $E^2$ . The fringe spacing is given by the angle which produces a change of one wavelength in the path-length difference.

The phase path-length difference  $(B/\lambda) \cos \theta$  can be more generally written as  $\mathbf{B} \cdot \mathbf{s}$ , where  $\mathbf{B}$ , the physical spacing, is equal to the element separation in wavelengths and its direction is that of the line joining the elements.\* The direction to the source is given by the unit vector  $\mathbf{s}$ . Equation (10.4) then becomes

$$R(t) \propto S \cos (2\pi \mathbf{B} \cdot \mathbf{s}(t)) \quad (10.5)$$

The interference response of a two-element interferometer can be pictured as a set of *fixed* quasi-sinusoidal fringes in the sky. The fringes are a function only of the interferometer separation. As the Earth rotates, a radio source travels through the fringe pattern (*i.e.*,  $\theta$  is a function of time), producing a quasi-sinusoidal response with a period determined by how quickly the term  $\mathbf{B} \cdot \mathbf{s}(t)$  varies with time. Usually the antennas track the radio source (*i.e.*, follow the radio source in its diurnal motion) so that maximum sensitivity is obtained from the desired radio source. A graph of fringe sizes and other parameters associated with an interferometer are given in Appendix I at the end of this chapter.

#### b) Fringe-Source Geometry

In order to describe aperture synthesis which makes use of the Earth's rotation, it is necessary to determine the fringe-source geometry. The forms of the necessary formulae are complicated and depend on the adopted coordinate system. The general relations will be derived here, and a list of the useful, working formulae are given in Appendix II.

\* In order to avoid ambiguity, the baseline direction will be defined as a vector from telescope 2 toward telescope 1.

A useful quantity in interferometry is the projected spacing  $\mathbf{b}$  of the physical baseline  $\mathbf{B}$  as viewed from a radio source. The change of the projected spacing due to the rotation of the Earth is illustrated using Figure 10.2. The Earth is pictured as viewed by an observer at the radio source, and the projection of the baseline clearly changes as the Earth rotates. In this example of an interferometer oriented in the east-west direction the projected baseline appears to rotate  $180^\circ$  in a 12-hour period.

Mathematically, the projected spacing  $\mathbf{b}$  is given by

$$\mathbf{b} = \mathbf{s} \times (\mathbf{B} \times \mathbf{s}) = \mathbf{B} - (\mathbf{s} \cdot \mathbf{B})\mathbf{s} \quad (10.6)$$

and is equal to the physical baseline  $\mathbf{B}$  less the component of  $\mathbf{B}$  in the direction of the source, *i.e.*,  $\mathbf{b}$  is the projection of the physical baseline perpendicular to the source direction. Generally, the projected spacing is resolved into components along directions to the east and north, which are commonly denoted  $u$  and  $v$ , respectively. The resultant path described in the “ $(u-v)$ ” plane produced as a source is tracked and is useful in understanding the methods of aperture synthesis. Equations and examples of  $(u-v)$  paths are shown in Appendix II.

#### c) Response to an Extended Source

The response of a two-element interferometer to an extended source can be obtained by considering the source to be a collection of point images and summing their individual responses. Let  $\mathbf{B}$  be the physical spacing of the interferometer and  $\mathbf{s}$  a convenient coordinate near the source. This point is denoted as the phase center. Any other point can be denoted by  $\mathbf{s} + \boldsymbol{\sigma}$ . If  $I(\boldsymbol{\sigma})$  describes the brightness distribution (angular distribution of power), then the response to the extended source is

$$R(t) = \int d\boldsymbol{\sigma} I(\boldsymbol{\sigma}) \cos [2\pi \mathbf{B} \cdot (\mathbf{s}(t) + \boldsymbol{\sigma})] \quad (10.7)$$

which is the response to a point source, Equation (10.5), integrated over the source. The flux density  $S$  of the source is equal to  $\int d\boldsymbol{\sigma} I(\boldsymbol{\sigma})$ . In most astronomical applications the radio source is followed in its diurnal

motion by each antenna (tracked) so that  $I(\boldsymbol{\sigma})$  is constant.

The term  $I(\boldsymbol{\sigma})$  is the brightness distribution as modified by the primary response (or beam pattern) of the individual antennas. If  $A(\boldsymbol{\sigma})$  is the primary response and  $I'(\boldsymbol{\sigma})$  the real brightness distribution, then

$$I(\boldsymbol{\sigma}) = I'(\boldsymbol{\sigma}) \cdot A(\boldsymbol{\sigma}) \quad (10.8)$$

See Section 10.3.1.

Since the angular size of the region observed is limited by the extent of the antenna response (typically less than one degree), the phase term in Equation (10.7) can be expanded to first order for sufficient accuracy.

$$\begin{aligned} \mathbf{B} \cdot (\mathbf{s} + \boldsymbol{\sigma}) &\simeq \mathbf{B} \cdot \mathbf{s} + \mathbf{B} \cdot \boldsymbol{\sigma} \\ &= \mathbf{B} \cdot \mathbf{s} + \mathbf{b} \cdot \boldsymbol{\sigma} \end{aligned} \quad (10.9)$$

Since  $\boldsymbol{\sigma}$  is nearly perpendicular to  $\mathbf{s}$ , only the projected spacing  $\mathbf{b}$  is used in the second term of the cosine. The response becomes

$$R(t) = \int_{-\infty}^{\infty} d\boldsymbol{\sigma} I(\boldsymbol{\sigma}) \cos [2\pi \mathbf{B} \cdot \mathbf{s} + 2\pi \mathbf{b} \cdot \boldsymbol{\sigma}] \quad (10.10)$$

This may be expanded into

$$\begin{aligned} R(t) &= \cos(2\pi \mathbf{B} \cdot \mathbf{s}) \int_{-\infty}^{\infty} d\boldsymbol{\sigma} I(\boldsymbol{\sigma}) \cos(2\pi \mathbf{b} \cdot \boldsymbol{\sigma}) \\ &\quad - \sin(2\pi \mathbf{B} \cdot \mathbf{s}) \int_{-\infty}^{\infty} d\boldsymbol{\sigma} I(\boldsymbol{\sigma}) \sin(2\pi \mathbf{b} \cdot \boldsymbol{\sigma}) \end{aligned}$$

However, it is much easier to work with the more compact complex form

$$\begin{aligned} R(t) &= \exp\{i2\pi \mathbf{B} \cdot \mathbf{s}(t)\} \int_{-\infty}^{\infty} d\boldsymbol{\sigma} I(\boldsymbol{\sigma}) \exp\{i2\pi \mathbf{b} \cdot \boldsymbol{\sigma}\} \\ &= V \exp\{i2\pi \mathbf{B} \cdot \mathbf{s}(t)\} \end{aligned} \quad (10.11)$$

where

$$V = \int_{-\infty}^{\infty} d\boldsymbol{\sigma} I(\boldsymbol{\sigma}) \exp\{i2\pi \mathbf{b} \cdot \boldsymbol{\sigma}\}$$

and where the real part of the right-hand side is implied. The exponential term outside of the integral is identical to Equation (10.5), the response of a point source located at the phase center. The integral, denoted as the visibility

function  $V$ , is a complex number and gives the interference of the source. The amplitude of  $V$  is proportional to the amplitude of the fringe pattern and the argument of  $V$  equals the phase shift in the fringe pattern from that of the response to a point source at the phase center.

From the form of Equation (10.11) the visibility function is obviously the Fourier transform of the brightness distribution. For a simple extended source, such as a double, the visibility function has a simple dependence on the projected spacing, and the separation and relative strengths of the two components of the double may be found by fitting such a model to the observed visibility function. Visibility functions corresponding to simple models are given in Appendix III. For more complicated sources the emission may be recovered from the observed response by performing the inverse Fourier transform

$$I(\boldsymbol{\sigma}) = \int_{-\infty}^{\infty} d\mathbf{b} V(\mathbf{b}) \exp\{-i2\pi \mathbf{b} \cdot \boldsymbol{\sigma}\} \quad (10.12)$$

Such a transform would be straightforward if the visibility function could be measured at all projected spacings. This is impossible, and the methods for extracting  $I$  from  $V$  for incomplete and discrete coverage are discussed in Section 10.4. Since the brightness distribution is a real function,  $I^*(\boldsymbol{\sigma}) = I(\boldsymbol{\sigma})$ , where (\*) denotes the complex conjugate. It is easily shown that  $V(-\mathbf{b}) = V^*(\mathbf{b})$ . That is, we need only measure the visibility function over half of the projected spacing plane.

It is common to use a Cartesian coordinate system, moving at the diurnal rate, in the neighborhood of the source. Let  $\mathbf{s} = (\alpha, \delta)$  and  $\boldsymbol{\sigma} = (x, y)$ , where  $x$  is an eastward displacement from  $\alpha$ , and  $y$  is a northern displacement from  $\delta$ . With such a coordinate system, and the convention that the phase increases for a source displacement toward the north and east, we get

$$V(u, v) = \int dx \int dy I(x, y) \exp\{+i2\pi(ux + vy)\} \quad (10.13)$$

$$I(x,y) = \int du \int dv V(u,v) \exp \{-i2\pi(ux+vy)\} \quad (10.14)$$

The effect of the curvature of the sky plane is generally insignificant.

#### d) Effect of Bandwidth

For most astronomical applications wide-frequency bandwidths are desired to increase the signal-to-noise ratio. The response of a two-element interferometer with a frequency response given by  $\alpha(\omega)$ , the bandwidth function, can be obtained from Equation (10.4):

$$R(t) \propto S \int d\omega \alpha(\omega) \cos(\omega\tau) \quad (10.15)$$

where  $\omega\tau = 2\pi\mathbf{B}\cdot\mathbf{s} = 2\pi(B/\lambda) \cos\theta$ . If the bandwidth function extends over  $\Delta\omega$  where  $\Delta\omega > 1/\tau$ , then the path-length change across the frequency band is sufficient to cause a loss of correlation.

Coherence across the frequency band is achieved by the insertion of time delay  $\tau_D \approx (B/c) \cos\theta$  in one or both arms of the interferometer to approximately equalize the path-length over both paths to the multiplier. The amount of delay must be changed to compensate for the variation of the geometric delay as the source is tracked. Each change of delay produces a phase jump in the output. In the simple interferometer in Figure 10.3 a continuously varying delay which exactly compensates for the geometric delay would lead to a constant response. A more detailed description of delay tracking and its effects is given in Section 10.2.

#### e) Interferometric Polarimetry

In general, radiation is polarized and the measurement of the polarization parameters is important in the understanding of the emission mechanisms. A description of polarized radiation is given by Chandrasekhar (1950), Cohen (1958), and Kraus (1966), and the application to interferometry is elucidated by Morris, Radhakrishnan, and Seielstad (1964), Conway and Kronberg (1969), and Weiler (1973). The electric field associated with a beam of monochromatic radiation of angular frequency  $\omega$  can be written as

$$\mathbf{E} = \hat{\mathbf{e}}_x Ex \cos(\omega t) + \hat{\mathbf{e}}_y Ey \cos(\omega t - \delta) \quad (10.16)$$

where  $Ex$  and  $Ey$  are the electric field amplitudes in the  $x$  and  $y$  directions ( $\hat{\mathbf{e}}_x, \hat{\mathbf{e}}_y$ ) and  $\delta$  is the phase difference between the two orthogonal modes. Any receptor of radiation (feed) is sensitive to only one of the two orthogonal modes of radiation [Equation (10.16) is only one of a possible set of these modes] and thus intercepts only that component of the radiation.

The radiation is coherently polarized if  $Ex$ ,  $Ey$ , and  $\delta$  remain constant over a long period of time. However, the radiation from most celestial objects is produced by a large number of independent radiators, and the resultant electric field from the ensemble varies randomly with time.

However, the fluctuations of  $Ex$  and  $Ey$ , although random, may be correlated. Such a beam of radiation is said to be polarized. For example, the synchrotron radiation emitted by a collection of electrons confined to planar orbits is partially polarized. The electric field for a noncoherent partially polarized beam of radiation written in vector complex form can be described by four parameters:

$$\mathbf{E} = \{\hat{\mathbf{e}}_x Eo (\cos\beta \cos\chi - i \sin\beta \sin\chi) + \hat{\mathbf{e}}_y Eo (\cos\beta \sin\chi + i \sin\beta \cos\chi) + \mathbf{Eu}\} e^{i\omega t} \quad (10.17)$$

where  $Eo$  is the amplitude of the electric field of the polarized radiation,  $\beta$  is the ellipticity,\* and  $\chi$  is the position angle. The amplitude of the unpolarized part of the radiation is  $\mathbf{Eu}$ ; its phase and direction are random. The parameters  $Eo$ ,  $\beta$ , and  $\chi$  can be written in terms of  $Ex$ ,  $Ey$  (here  $Ex$  and  $Ey$  refer only to the polarized part of the radiation), and  $\delta$  in Equation (10.16) (see Chandrasekhar, 1950, p. 26).

The characteristic of partially polarized noncoherent radiation is most commonly

\* If  $\beta > 0$ , the radiation is said to be left-hand elliptically polarized. If  $\beta < 0$ , it is right-hand elliptically polarized. Left-hand polarization means a clockwise rotation of the electric vector with the wave approaching.

described in terms of the four Stokes intensity parameters  $I$ ,  $Q$ ,  $U$ , and  $V$ . These are defined by the following relations:

$$\begin{aligned}
 I &= \text{total intensity of radiation} \\
 &= \langle E_o^2 \rangle + \langle |Eu^2| \rangle \\
 &= \langle Ex^2 \rangle + \langle Ey^2 \rangle + \langle |Eu^2| \rangle \\
 Q &= \text{linearly polarized intensity} \\
 &= \langle E_o^2 \rangle \cos 2\beta \cos 2\chi \\
 &= \langle Ex^2 \rangle - \langle Ey^2 \rangle \\
 U &= \text{linearly polarized intensity} \\
 &= \langle E_o^2 \rangle \cos 2\beta \sin 2\chi \\
 &= \langle Ex Ey \rangle \cos \delta \\
 V &= \text{circularly polarized intensity} \\
 &= \langle E_o^2 \rangle \sin 2\beta \\
 &= \langle Ex Ey \rangle \sin \delta
 \end{aligned} \tag{10.18}$$

The Stokes parameters are defined in terms of r.m.s. time averages of the electric field components.

The response to the radiation will depend on the orientation and ellipticity of the feed. A dipole parallel to the  $x$ -axis will respond only to the  $x$ -component of the radiation and measures  $\frac{1}{2}(I + Q)$ . Rotation of the dipole to the  $y$ -direction will change the response to the  $y$ -component of the radiation and measure  $\frac{1}{2}(I - Q)$ .

The response of an interferometer with arbitrary feed characteristics can also be expressed in terms of Stokes parameters, and specific examples are also given in Appendix IV. Since all the Stokes parameters are intensity parameters, the brightness distribution of  $Q(\sigma)$ ,  $U(\sigma)$ , and  $V(\sigma)$  can be found in the same way as the total intensity,  $I(\sigma)$ . In most cases we will discuss explicitly the interferometry of the total intensity, but the term  $I(\sigma)$  can be replaced by a sum of the various Stokes parameters  $F(I, Q, U, V; \sigma)$  where  $F$  depends on the feed configuration.

## 10.2 A Working Interferometer

### 10.2.1 A Complete System

A block diagram of a working interferometer and the response of the system are shown

in Figure 10.4. The diagram is complex and includes the major components of a complete system. The response in mathematical terms to incoming radiation at various stages is shown. Only the phase behavior of the system is incorporated into the equations. The gain factors for the system are neglected. Error terms related to cable length changes, temperature effects, etc., have not been included.

The major difference from the simplified system in Figure 10.3 is the conversion of the observed radio frequency (RF) to an intermediate frequency (IF) using a standard heterodyne process with a coherent local oscillator (LO). With this conversion most of the path over which the signals are joined is at a moderately low frequency, where cable losses are smaller, path-length changes due to external variations are smaller, and electronic components are less expensive. In addition, a change of observing frequency requires only a change of components in front of the heterodyning stage and in the LO frequency.

A description of the technical aspects of an interferometer has been given by Read (1963) and Swenson (1969) and will not be repeated here. Some obvious requirements and the function of various components are given below:

- (1) A low-noise RF amplifier. The sensitivity of most systems is limited by the noise generated in the RF amplifier. A large gain is also desirable to decrease the effect of noise generated by following stages.
- (2) A stable heterodyne process. The RF signal is converted to an IF signal by mixing (multiplying) the RF signal with a strong LO signal. In order to preserve the RF signal characteristics in the IF signal, the LO signal must be monochromatic and the phase relationship of the LO signal at each mixer must be coherent. Coherence is difficult to obtain over a distance of more than  $\sim 10$  km. A term  $\phi(t)$  has been included in the LO signal sent to the mixer of antenna #2. Phase errors in the interferometer system and system modifications such as lobe rotation can be

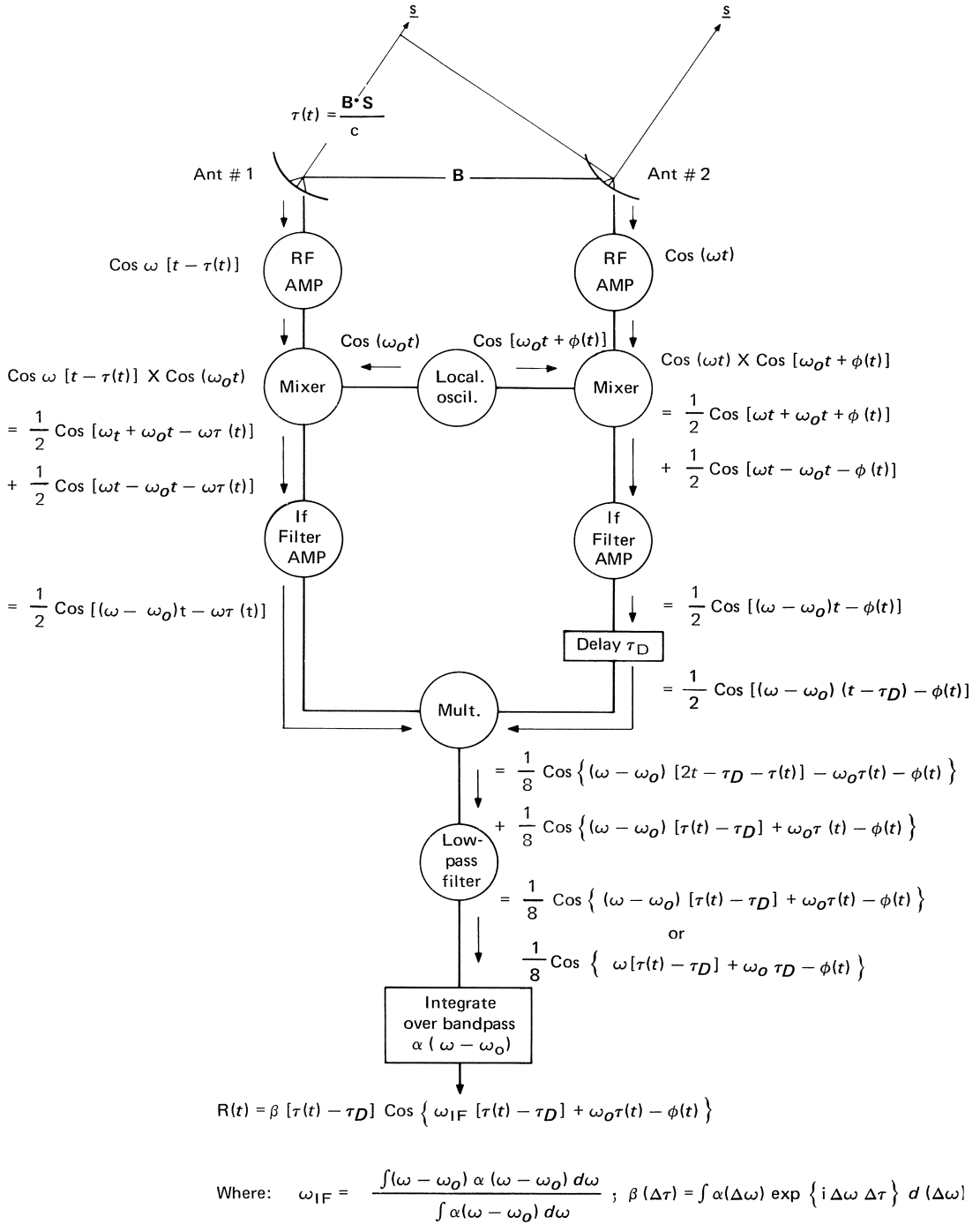


Figure 10.4 The schematic working diagram of the response of an interferometer.

understood in terms of the behavior of  $\phi(t)$ . With a heterodyne process two RF frequencies (sidebands) are superimposed when converted to an IF frequency  $\omega_{IF}$ . The upper sideband has a frequency of  $\omega_o + \omega_{IF}$ , and a lower sideband has a frequency of  $\omega_o - \omega_{IF}$ . For many astronomical applications both sidebands are used; however, one sideband may be rejected by placing an appropriate filter in the RF line.

- (3) IF system. Amplification is needed to increase the signals for subsequent processing. A filter is also needed to reject the high-frequency signal and to limit the IF frequency range within the specifications of the multiplier, delay lines, and IF amplifier bandpass. For spectral line work, narrow-band filters may also be present. A variable delay line, usually consisting of a binary series of lengths of cable, is placed in one or both of the IF lines to equalize the travel time of the radiation via the two possible paths. The insertion of delay  $\tau_D$  is shown in the response of antenna #2.
- (4) Multiplication and terminal processing. The signals from each antenna are multiplied and the high-frequency response  $(\omega - \omega_o)2t$  is rejected by a low-pass filter. The subsequent monochromatic response is given in two forms in Figure 10.4.

### 10.2.2 Bandwidth Effects

#### a) Response

The response after multiplication and filtering is that for a monochromatic signal within the system bandwidth. The bandwidth is usually determined by IF filtering, but can be affected by a limited bandwidth in any part of the system. If the bandwidth function of the response is denoted by  $\alpha(\omega - \omega_o)^*$  (a complex quantity), the resulting response is given at the bottom of Figure 10.4. The average IF fre-

\* The term  $\alpha(\omega - \omega_o)$  is the bandwidth of the system in terms of the input RF frequencies. For a double sideband system  $\alpha(\omega - \omega_o)$  extends above and below the LO frequency  $\omega_o$ , although the sidebands are folded together in the IF conversion.

quency weighted by the bandwidth function is  $\omega_{IF}$ . The term  $\beta(\tau_D - \tau(t))$  is called the fringe washing function and is the complex Fourier transform of  $\alpha(\omega - \omega_o)$ ; see Appendix V.

#### b) Delay Tracking

We have already alluded to the loss of coherence over a large bandwidth in Section 10.1. The difference in the time of travel from the source via the two possible paths  $\Delta\tau \equiv \tau_D - \tau(t)$  must be made smaller than the reciprocal bandwidth; otherwise  $\beta(\Delta\tau)$  will be significantly less than unity. At present there is no technically feasible method for obtaining a continuously variable delay line; a binary array, usually driven by a computer, sets  $\tau_D \approx \tau(t)$  within the stepping interval of the delay. Unfortunately, in a single sideband system a discrete change of  $\tau_D$  produces a phase jump equal to  $\omega_{IF} \Delta\tau$  in the response, which disturbs the sinusoidal output. Three solutions are possible: (1) Change  $\tau_D$  in steps of  $2\pi/\omega_{IF}$  so that all of the phase jumps are  $2\pi$  at the center of the IF band. However, significant losses occur unless the bandwidth is much less than  $\omega_{IF}$ . (2) Change  $\tau_D$  in very small steps so that each phase jump is small. (3) Compensate for the phase change due to the delay step in the IF line by a phase-adding device.

For observations of continuum radiation where there is no fundamental difference between the two sidebands, the use of a double sideband system avoids the problem of phase jumps caused by delay tracking. The phase jump for each sideband is in the opposite direction and hence they cancel each other for a double sideband system, *i.e.*,  $\omega_{IF} = 0$  for a balanced double sideband system.

### 10.2.3 Calibrations

The complete response  $R(t)$  of a two-element interferometer to an extended source of radiation (see Equation 10.11) is

$$R(t) \sim Re \{ \beta(\Delta\tau) V(\mathbf{b}) \exp i\{2\pi\mathbf{B} \cdot \mathbf{s}(t) + \phi(t)\} \} \tag{10.19}$$

where  $\beta$  is the fringe washing function,  $\Delta\tau$  is the time delay difference in the two paths

$[\tau_D - \tau(t)]$ ,  $V$  is the visibility function,  $\mathbf{b}$  is the projected baseline,  $\mathbf{B}$  is the physical baseline,  $\mathbf{s}(t)$  is the unit vector to the source, and  $\phi(t)$  is a phase term containing lobe rotation and other deliberate phase modifications as well as random phase errors. In this section we shall assume that the delay is accurately tracked and that  $\beta$  is unity.

The response and the precise time as well as other useful parameters are sampled by a computer, and the apparent visibility function is determined by fitting the response to the form  $\exp i\{2\pi\mathbf{B}\cdot\mathbf{s}(t)\}$ . The apparent visibility function must then be corrected for certain instrumental effects.

Nearly all corrections to the observed response are determined by the use of radio sources known as calibrators. Generally these are point sources (a source of emission with an angular size much less than a fringe separation) of known flux density, position, and polarization. The calibrators are observed periodically, and certain system parameters are adjusted so that the correct values of flux density, polarization, and zero phase are obtained for these sources. The same (or interpolated) adjustments are made to all observations, *i.e.*, the apparent visibility functions are corrected in the same way. There are four basic calibrations for continuum measurements to determine the instrumental parameters: gain, baseline, phase, and polarization.

The gain calibration is the determination of the ratio of the flux density of the calibrators to the correlated amplitude of the response. All of the electronic components shown in Figure 10.4 have some variation of gain with time, and the observation of a source of known flux density every few hours or days (depending on the overall gain stability of the system) is needed to follow the variations. Often the system is equipped with an automatic level control which holds the IF power constant at some late stage of the system. An increase in the system noise temperature then leads to a reduction in the amplitude of the signals, and observation of calibrators is still required to monitor ampli-

tude fluctuations. Other systematic gain changes must be applied before a satisfactory time dependence of gain can be obtained, such as the effects of the filter responses, atmospheric attenuation, antenna efficiency as a function of elevation, added system noise temperature due to a strong source or ground radiation pick-up, and loss of coherence with various delay elements. Determination of the gain to an accuracy of several percent is frequently achieved.

An *a priori* baseline  $\mathbf{B}$  is used to fit the interferometer response to a computed fringe pattern. The baseline cannot be surveyed accurately enough [better than (1/100) of a wavelength] and must be determined by the calibration process. Point sources of accurately known position are observed over a wide range of hour angle and declination, and the systematic variation of the visibility phase response with hour angle and declination is used to determine a more accurate baseline value. Phase drifts in the system response and errors in the assumed source positions are detrimental to a good baseline determination.

The baseline separation between two telescopes is equal to the vector joining their respective phase centers, which are usually near the focal points of the telescopes. Most telescopes are built with intersecting axes of motion so that the phase center remains at a fixed distance from the intersection regardless of the pointing direction. Thus, the baseline separation  $\mathbf{B}$  is independent of the pointing position. Even if the antennas are moved slightly off position, the phase center defined by the source radiation does not move. The amplitude of the response to the source will decrease, but the phase of the sinusoidal response is unaltered. For nonidentical antennas with nonintersecting axes, the baseline separation is a function of source direction. The geometry has been worked out by Wade (1970) for a nonintersecting equatorial mount.

For telescopes with intersecting axes, the baseline error is due to the uncertainties in the mutual positions of the antennas. Since many arrays use moveable antennas, exact positions cannot be determined beforehand.

From Equation (10.19) the expected variation in phase over the sky is  $\Delta\mathbf{B}\cdot\mathbf{s}$ , where  $\Delta\mathbf{B}$  is a constant. Observations of at least four sources, and preferably several tens of sources for adequate redundancy, are needed to determine the three coordinates of  $\Delta\mathbf{B}$  and a phase offset.

Once an accurate baseline separation has been obtained, the phase behavior (after known phase modifications are considered) of the system  $\phi(t)$  can be followed by observing calibrators as often as necessary.

Before the above phase calibrations can be made, systematic phase variations due to the delay in the atmosphere must first be considered. If the antennas are at different elevations, the two radiation paths go through different amounts of atmosphere, causing a phase change as a function of source position and ground weather conditions. The resultant phase correction, which depends on the refractive index, can be calculated. In the plane-parallel approximation the troposphere produces no additional phase change. Although the position of a source can be changed by many arc minutes by refraction, the phase path length between the two telescopes is unaffected. For observations at low elevation, the spherical nature of the troposphere must be considered, and a phase correction dependent on gross atmospheric properties is needed. This correction is significant for element separations greater than  $\sim 1$  km (Hinder and Ryle, 1971), corresponding to a typical tropospheric scale size. Also, short-term phase fluctuations occur, mainly due to water vapor, which gives rise to path-length changes of a few millimeters. These short-term fluctuations are due to small-scale irregularities of size  $\lesssim 1$  km and cannot be effectively calibrated.

The polarization response  $F(I, Q, U, V; \sigma)$  of an interferometer is given in Appendix IV. The feed alignment and ellipticity cannot be accurately measured, so observations of calibrators with known polarization values are used. The details of the calibration process depend on the type of polarization desired and the feed configurations. The polarization

response also varies over the primary beam and can be calculated in some cases and may vary somewhat with the telescope pointing.

#### 10.2.4 Modifications to the Basic Interferometer

There are many modifications to the basic interferometer system. Some systems use several intermediate frequencies, each produced by an independent local oscillator. This is often done for convenience (*e.g.*, using a 300-MHz IF system with delays designed for 10 MHz), but is also used to adjust the output in a prescribed manner. Many systems use complicated LO chains for greater frequency versatility and phase-compensating systems. Four modifications—lobe rotation, spectral-line interferometry, very-long-baseline (VLB) interferometry, and intensity interferometry—will be discussed in some detail.

##### a) Lobe Rotation

The frequency of the interferometer response (the fringe frequency) can be considered as the carrier frequency for the signal (the visibility function). The rate of change of the visibility function is proportional to the rate of change of the projected spacing, whereas the fringe rate is proportional to  $u$ , the east-west projected spacing. At times the fringe frequency is less than that associated with the visibility change and information can be lost. Also, the variation of the fringe frequency with baseline separation and source position is a nuisance in the data analysis; the frequency dependence of the system must be accurately calibrated and the data must be sampled at least two times a fringe period.

One method of arbitrarily changing the fringe frequency is the addition of a varying phase, usually controlled by a computer, to one side of the interferometer. The additional phase can be added in the RF, LO, or IF lines using a phase rotation capacitor device or by a deliberate offset of the local oscillator signal to one antenna (Read, 1963). The response then

has the time dependence

$$\cos(2\pi\mathbf{B}\cdot\mathbf{s}(t) + \phi(t)) \quad (10.20)$$

Often  $\phi(t)$  is set equal to  $-2\pi\mathbf{B}\cdot\mathbf{s}(t) + \Omega t$ , where  $\Omega$  is the constant fringe frequency, independent of baseline or source position. For multi-element arrays it is not possible to obtain the same fringe frequency for all correlated pairs, although the time-dependent term can be subtracted. The Westerbork synthesis telescope in the Netherlands uses a system in which the fringe rate is zero. Special switching techniques are then necessary to avoid a slow drifting of the response and to measure the real and imaginary parts of the visibility function (Casse and Muller, 1973).

### b) Spectral-Line Interferometry

The discovery of many radio-frequency lines has made spectral-line interferometry necessary in order to achieve high angular resolution, especially for low-frequency lines. The frequency (velocity) dependence of many sources of line radiation is complicated, and complete observations require many channels of narrow bandwidths (1 kHz to 1 MHz) to adequately cover the relevant radiation.

Two methods are used to obtain high spectral resolution. First, two sets of matched filters are introduced, one into each IF line (see Figure 10.5a). Each filter produces a separate output, which is individually multiplied with the other matched filter (Rogstad *et al.*, 1967). The response of each filter pair is identical to that of a broad-band interferometer and is a direct measure of the visibility function averaged over the filter bandwidth.

Another method of obtaining high spectral resolution uses the multiplication of the broad-band signal with many large delay intervals (Baldwin *et al.*, 1971). The analogue procedure is shown in Figure 10.5(b). The output from each correlator is proportional to  $\beta(k\Delta\tau)$ ,  $k = -N \leq 0 \leq N$ , where  $\Delta\tau$  is the delay interval step and  $N\Delta\tau$  is the total delay range in the correlation. Since the bandpass is the Fourier transform of the fringe washing function  $\beta$ , the bandpass with respect

to  $\omega_{\text{IF}}$  may be recovered as

$$\alpha(l\Delta\omega) = \sum_{k=-N}^N \beta(k\Delta\tau) \exp\{i\pi lk/N\};$$

$$-N \leq l \leq N \quad (10.21)$$

The resolution is  $\Delta\omega \approx (N\Delta\tau)^{-1}$  and the aliasing frequency is  $\omega_A \approx \Delta\tau^{-1}$ ; so that the response is given by

$$\alpha'(\omega) = \sum_{n=-\infty}^{\infty} \alpha(\omega + n\omega_A)$$

where  $n$  is an integer. The aliasing can be avoided by placing filters in the IF lines to limit the IF bandwidth range to less than  $\omega_A$ . The filter shape corresponding to the simple sum in Equation (10.21) is

$$\frac{\sin(N\Delta\tau\omega)}{(N\Delta\tau\omega)} \quad (10.22)$$

This filter has the undesirable property of high sidelobes. Convolution with a Gaussian function [produced by multiplying  $\beta(k\Delta\tau)$  by a Gaussian] or hanning will reduce the side-lobe level but increase the resolution size  $\Delta\omega$ .

The same procedure can be obtained from a digital cross-correlator. Several seconds of IF signals from each element are stored and subsequently multiplied with various time-delay offsets  $\Delta\tau$  to obtain  $\beta(k\Delta\tau)$ .

Normal operation of the spectral-line interferometer is single sideband. The rejection of one sideband is usually obtained by a bandpass filter in the RF line of each antenna. The bandpass of  $\alpha(\omega)$  is the product of the system bandpass and the radiation from the source. The system bandpass can be measured experimentally or determined from observations of a calibrator source with no line radiation in the frequency range.

An interesting technique for spectral-line observations is that of a double sideband system operating with a deliberate delay offset so that the two sidebands cancel (Radhakrishnan *et al.*, 1971). This occurs when  $\beta(\tau_D - \tau(t)) = 0$ . If the upper and lower sidebands are identical in frequency characteristics and the delay tracking is accurate, the

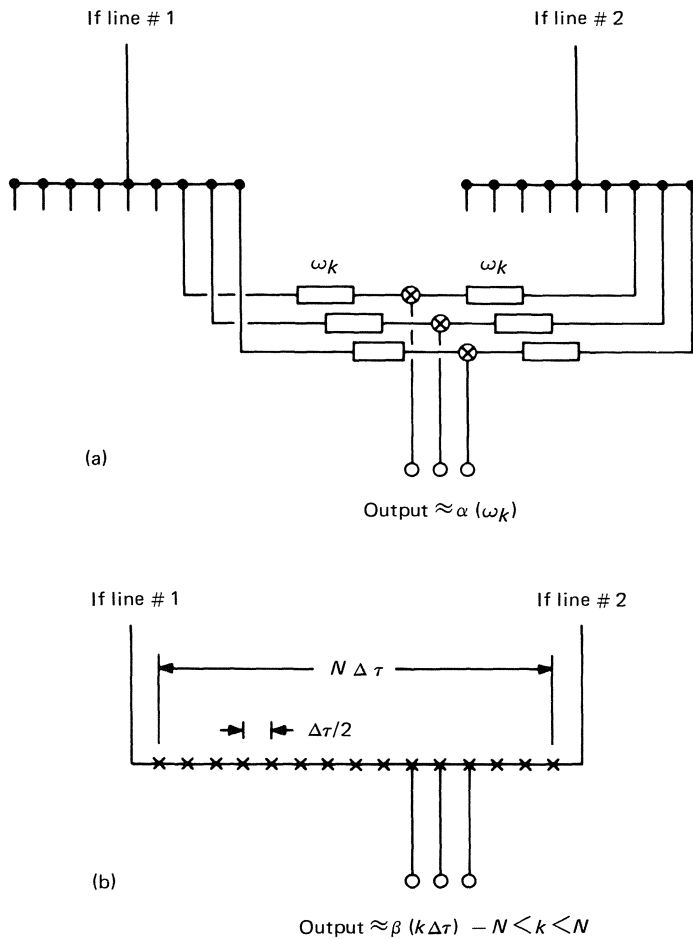


Figure 10.5 Spectral-line receivers. (a) A conventional filter bank receiver. (b) Cross-correlation spectrometer with correlation at various delay intervals.

output response is proportional to the difference of radiation between the two sidebands. The result is a null experiment, unless there is line radiation in either sideband.

c) Very-Long-Baseline Interferometry

As baselines are increased, the major problem is the maintenance of LO stability between the elements. Over moderate distances of about 100 km, radio links have been used to transport the local oscillator signals and IF responses. However, unless sophisticated path-length compensation schemes are

used, the phase change  $\phi(t)$  of the response can vary unpredictably (Elgaroy *et al.*, 1962; Basart *et al.*, 1970).

For very-long-baseline (VLB) interferometry independent local oscillators are used at each element. This technique is now possible, with the advent of very accurate frequency standards which use the discrete atomic energy transitions (cf. Cohen, 1969). In order to obtain a phase stable response, the error in the LO phase,  $\phi(t)$ , must remain constant within a radian. For observations at 10 cm, for example, stability over 15 minutes

requires an oscillator stability of 1 part in  $3 \times 10^9 \text{ Hz} \times 10^3 \text{ sec} \approx 1$  part in  $10^{12.5}$ . Such stability can be obtained using hydrogen masers as frequency standards.

The IF output of each element is recorded separately on a high-speed analogue or digital recording device. Systems are currently available in which  $10^7$  bits of information can be recorded each second, thereby permitting bandwidths of several megahertz to be properly sampled. The two IF responses are then multiplied in a digital computer or on a special analogue device. The IF responses must be lined up with the proper time delay before multiplication. This requires a timing accuracy of about  $10^{-6}$  sec for a bandwidth of 1 MHz. Otherwise, the fringe washing function  $\beta(\tau_D - \tau(t))$  will be much less than 1.

For the reduction of VLB data the observed response is fitted to the form of Equation (10.19) in the same way as a conventional interferometer. Because of baseline inaccuracies, source position errors, timing errors, and oscillator drift, the delay may be significantly in error, causing loss of correlation. Also, error in the calculated fringe rate may limit the integration time. The response is therefore fitted using a range of delay offsets and fringe frequencies around the nominal values. The maximum amplitude obtained is proportional to the visibility amplitude of the source. The visibility phase can be measured only when baseline errors and clock drifts are also accurately determined.

A systematic analysis of the fringe frequency and the time-delay measurements for observations of sources can be used to obtain a more accurate baseline separation and improved source positions. Such an analysis is described by Cohen and Shaffer (1971) using an equation similar to that given in the Appendix for the fringe frequency and time delay. Two modifications are needed. Firstly, since the time delay is many milliseconds between two distant telescopes, there is a substantial change of the baseline separation during this time. A "retarded" rather than an instantaneous baseline must be used. Secondly, a relativistic correction caused by the

large mutual velocity of the telescopes is necessary. Source positions of 0.1 arc second accuracy are now being obtained by using the fringe frequency and time delay.

One method for improved accuracy of VLB interferometry is by the observation of several sources or frequencies simultaneously. The relative visibility functions among the sources or frequencies can be obtained even with inaccurate baselines and source positions, and sizeable oscillator drifts. Accurate maps of complicated regions of small-diameter OH and H<sub>2</sub>O emission regions have been obtained in this way (cf. Moran *et al.*, 1968). For continuum observations four-antenna experiments using two distant observatories, each with two antennas, have been successful. Two different sources are observed with each VLB interferometer, but the same local oscillator is used at each location, and the two responses are recorded simultaneously on the same device. Most of the gross baseline errors, oscillator errors, and position errors are cancelled by the technique.

The ultimate measurement of positions in the order of milliseconds of arc will require a careful calibration, understanding, and measurement of many effects: continental drift, Earth tides, precision rotation of the Earth, atmospheric and ionospheric path-length changes, and relativistic bending of radio waves. All of these effects are significant at the millisecond of arc level.

#### d) Intensity Interferometry

Hanbury Brown and Twiss (cf. Hanbury Brown, 1968) recognized that it is not necessary to have a phase stable system for an interferometer. In an intensity interferometer the RF signals from each antenna are mixed with two incoherent LO signals, with the resulting lack of phase stability in the IF signals. The separate signals are each detected and then multiplied together. Although no phase relationship exists between the two outputs, some correlation is obtained because of common intensity fluctuations in each output.

An analysis of the response for an inten-

sity interferometer has been given by Bracewell (1958) and MacPhie (1966). The response is proportional to the square of the visibility amplitude and all phase information is lost, although some phase behavior can be recovered with multi-element intensity interferometry.

The signal-to-noise ratio for an intensity interferometer is much lower than that for a correlating interferometer. The general formulae have been considered by Clark (1968). The loss of signal-to-noise is related to the bandwidth of the fringe power. For a correlating interferometer with perfect phase stability [*i.e.*,  $\phi(t) = 0$ ], all of the correlated power falls within a narrow frequency range ( $1/T$ ), where  $T$  is the length of the observation. Only the noise falling within that passband need be associated with the measurement. For an intensity interferometer the fringe power is spread over the entire frequency range of several megahertz determined by the detector and the resulting noise is thus much larger. Before the use of hydrogen masers as oscillator standards, the sensitivity of VLB observations was also limited because of random fluctuations in the phase stability, which broadened the fringe frequency range considerably.

### 10.3 Aperture Synthesis

#### 10.3.1 Filled and Unfilled Aperture Beams

In Section 10.1 we alluded to some of the different characteristics between the beam of a filled aperture and the beam of a synthesis instrument. Most of the differences are caused by incomplete and discrete coverage of the  $(u, v)$  plane with aperture synthesis instruments.

Most telescopes can be described in terms of an aperture plane on which currents are induced by the incoming radiation (Kraus, 1966, Chapter 6; Christiansen and Högbom, 1969, Chapter 3). The voltage pattern  $\mathcal{V}(\boldsymbol{\sigma})$  of the aperture plane is given by

$$\mathcal{V}(\boldsymbol{\sigma}) = \int_{\text{aperture}} d\mathbf{x} \exp\{-i2\pi\mathbf{x}\cdot\boldsymbol{\sigma}\} g(\mathbf{x}) \quad (10.23)$$

where  $\boldsymbol{\sigma}$  is the direction of the response with respect to the direction of the pointing axis. The term  $g(\mathbf{x})$  is the aperture distribution (grading) and gives the relative response over the aperture. The aperture distribution depends on the characteristics of the antenna surface and the illumination by the feed.

The power pattern  $A(\boldsymbol{\sigma}) \equiv \mathcal{V}(\boldsymbol{\sigma})^2$  is given by

$$A(\boldsymbol{\sigma}) = \int d\mathbf{x} \exp\{-i2\pi\mathbf{x}\cdot\boldsymbol{\sigma}\} h(\mathbf{x}) \quad (10.24)$$

with

$$h(\mathbf{x}) \equiv \int d\mathbf{x}' g(\mathbf{x}') g^*(\mathbf{x} - \mathbf{x}') \quad (10.25)$$

where  $h(\mathbf{x})$  is called the transfer function. It is a measure of the density of mutual spacings in the aperture. An example of the above quantities for a filled-aperture radio-telescope is shown in Figure 10.6.

The above analysis is identical for an array; however, the aperture distribution is now produced by many spatially separated antennas, each associated with an element of the array. In the case of an array with a total set of mutual separations  $\mathbf{b}_j$ ,  $j = 1, \dots, N$  and with identical antennas each of grading  $g_A(\mathbf{x})$  and transfer function  $h_A(\mathbf{x})$ , the transfer function of the array is

$$h(\mathbf{x}) = \sum_{j=1}^N h_A(\mathbf{x} - \mathbf{b}_j) \quad (10.26)$$

and

$$P(\boldsymbol{\sigma}) = A(\boldsymbol{\sigma}) \sum_{j=1}^N \exp\{-i2\pi\mathbf{b}_j\cdot\boldsymbol{\sigma}\} \quad (10.27)$$

where  $P(\boldsymbol{\sigma})$  is the power pattern for the array and  $A(\boldsymbol{\sigma})$  is the power pattern for the elemental antenna.

The aperture functions for two linear arrays are also shown in Figure 10.6. The first array consists of seven identical equally spaced elements with an overall size equal to that of the filled aperture. The envelope of the shape of the transfer function is similar to that of the filled aperture and the central peaks of the power patterns are about the same width. The discrete spacings (stepping interval) of the array produce grating responses (images) that are attenuated by the

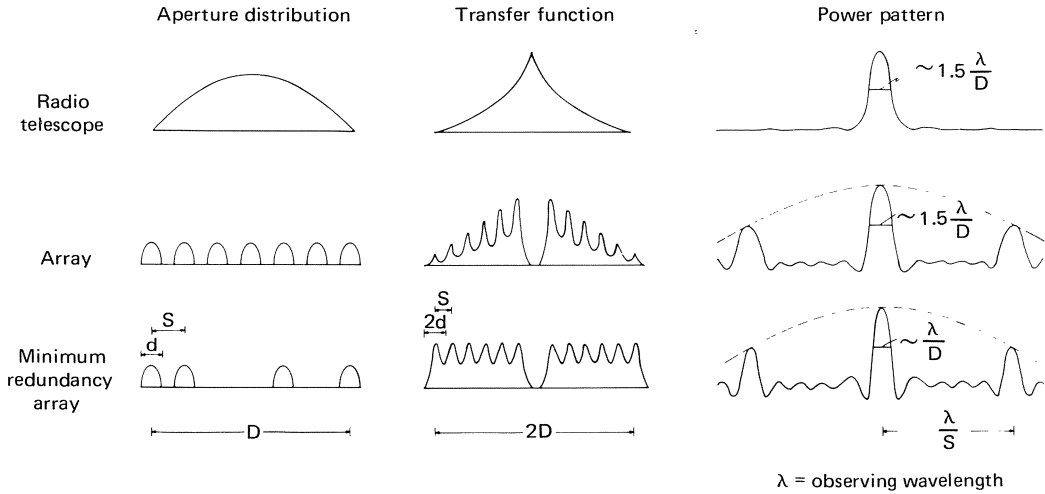


**Figure 10.6** The aperture distribution, transfer function, and power pattern for: (a) a radio telescope, (b) an array with equally spaced elements, (c) a minimum redundancy array (placing four elements in such a way so as to obtain six nonredundant spacings).

elemental power pattern. For a multiplying interferometer the zero spacing (self-correlating pairs) is not obtained.

The second array contains only four elements but they are placed in such a way that the same six mutual separations of the previous array are measured. This type of an array is called a minimum redundancy array (Moffet, 1968). The envelope of this transfer function is more uniform and corresponds to a filled aperture strongly illuminated at the edge. The central beamwidth is narrower than the previous array, but the sidelobe level [wiggles in  $P(\sigma)$ ] is larger because of the sharper cut-off in the transfer function. The grating response, a function of the stepping interval, is similar to the previous array.

Neglecting the power pattern of the individual elements, the synthesized beam of an array is

$$P(\sigma) = \sum_{j=1}^N \exp \{ -i2\pi \mathbf{b}_j \cdot \sigma \} w_j \quad (10.28)$$

or

$$P(x,y) = \sum_{j=1}^N \exp \{ -i2\pi(ux + vy) \} w_j \quad (10.29)$$

in rectangular coordinates. The weighting  $w_j$  of each data point has been incorporated into

the equations. If the data for each telescope pair are individually combined in a computer, the weighting may be chosen to modify the envelope of the transfer function. The optimum weighting depends on sidelobe level and signal-to-noise considerations.

The output of a synthesis array is a set of visibility functions  $V(u_j, v_j)$ , and the resultant brightness distribution (cf. Equation 10.14) is

$$I(x,y) = \sum_{j=1}^N V(u_j, v_j) \exp \{ -i2\pi(u_j x + v_j y) \} w_j \quad (10.30)$$

The synthesized beam is thus the brightness distribution obtained by observing a point source. The observed brightness distribution is the convolution of the true brightness distribution with the synthesized beam.

A skeleton array contains all of the desired mutual separations at any instant so that it is not necessary to track a radio source in order to obtain a reasonable synthesized beam. The visibility functions are then transformed to obtain the brightness distribution. For a primitive array the necessary baselines are obtained by moving some of the elements and/or utilizing the rotation of the Earth. For both types of arrays the properties of the synthesized beams are discussed in the next

section. Explicit illustrations of skeleton arrays and their responses are given in Christiansen and Högbom (1969).

The visibility functions are obtained by averaging the quasi-sinusoidal response of each interferometer pair. The averaging duration should not exceed the time for which the visibility function significantly changes. This depends on the angular size of the radio emission. The finite angular size imposed by the primary response of the individual elements limits the averaging time to several minutes for a 1-km baseline and a 25-m element size. The averaging time for observations of intense small-diameter sources may be considerably increased. A general practice is to average the visibility function of all baselines at equal intervals. Each sampled point then has about the same signal-to-noise although the smaller spacings in the array have been sampled more often than necessary.

### 10.3.2 Properties of a Synthesized Beam

A more detailed discussion of the properties of a synthesized beam is given in conjunction with Figures 10.7 and 10.8. In Figure 10.7 the coverage in the  $(u-v)$  plane is shown for a set of observations of CAS A. Each point represents an observation of a unit time interval—hence approximately unit weight. The interferometer baseline is not aligned east-west, causing a displacement of the  $(u-v)$  ellipses from the origin.

#### a) Beam-Weighting and Its Effects

The natural weighting (effective aperture distribution) for the array is proportional to the density of sampled points weighted in accordance to the signal-to-noise of each point. However, for most synthesis instruments we are at liberty to weight each observation as desired, since the summation of Equations (10.29) and (10.30) is usually done in a digital computer.

The synthesized beam and brightness distribution for Cas A with natural weighting are shown in Figure 10.8(a). If the outer spacings are more heavily weighted, the cor-

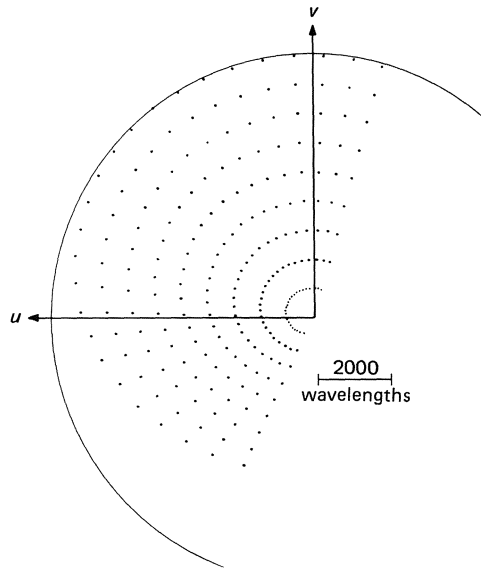


**Figure 10.7** The coverage in the  $(u-v)$  plane for observations of CAS A, using the NRAO interferometer. The source was tracked from hour angle  $-6^h$  to  $+6^h$  at baselines 100 to 900 m in 100-m intervals. Each point represents a 30-minute average of the data. In practice the averaging interval used is  $\frac{1}{2}$  minute.

responding beam and brightness distributions are shown in Figure 10.8(b). With this weighting the transfer function is  $u(\mathbf{x}) \approx 1$ , corresponding to a uniformly sampled aperture. The beamwidth is smaller but the sidelobes are higher. In Figure 10.8(c) the beam and brightness distribution with the inner spacings weighted more heavily is given. The synthesized beam width is increased but there is a decrease of the inner sidelobes.

#### b) Sidelobe Levels

At some angles signals from parts of the aperture add in phase to produce ripples in the power pattern. These ripples are similar to those of filled-aperture telescopes. Two major causes of sidelobes are (1) diffraction at the edge of the aperture and (2) gaps in the synthetic aperture coverage in the  $(u,v)$  plane. The inner sidelobes caused by the aperture edge can be decreased by lowering the weighting of the outer spacings so that the edge-like diffraction of the aperture extremities is

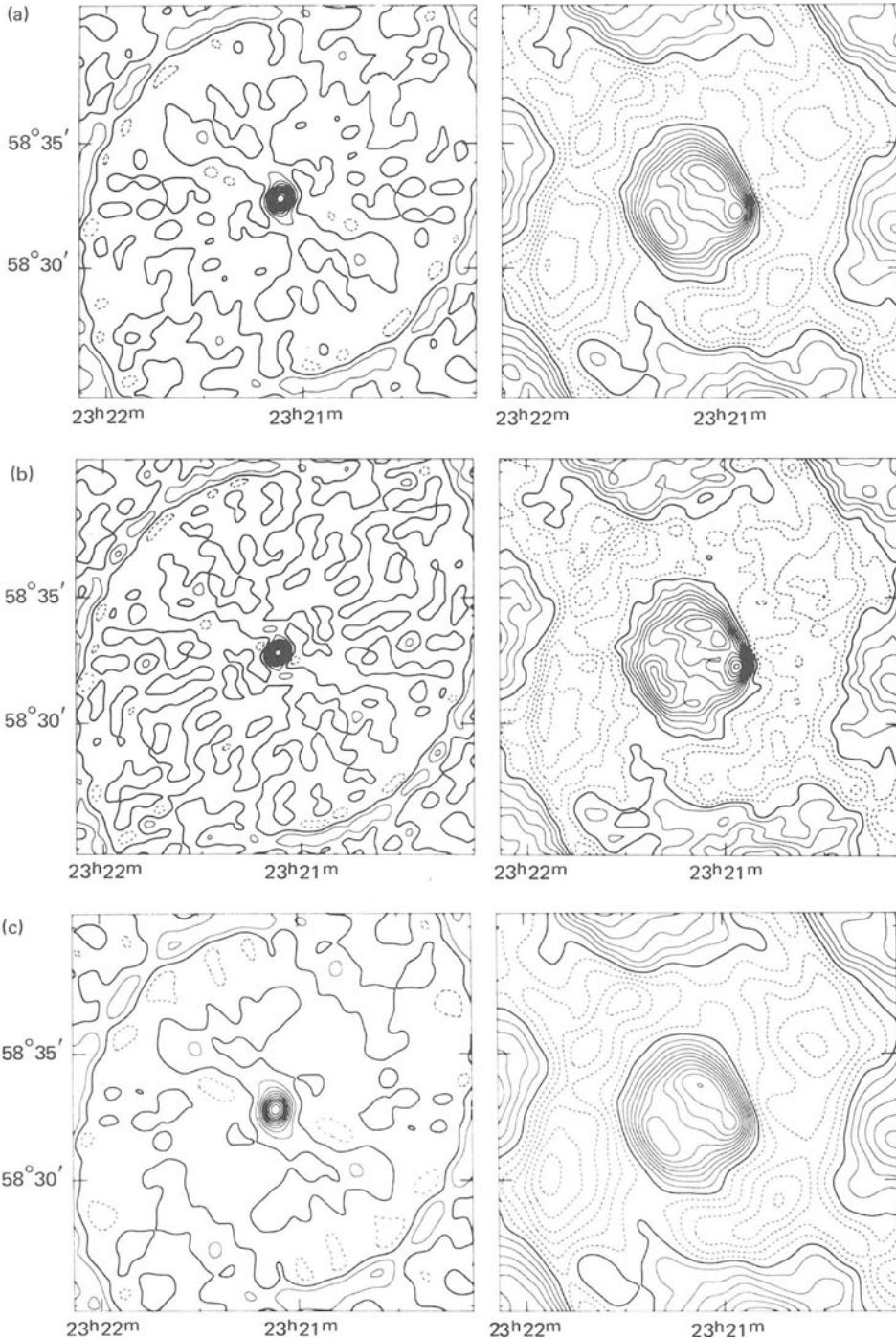


**Figure 10.8** The synthesized beam and brightness distribution for CAS A using the  $(u-v)$  coverage shown in Figure 10.7. Contours are at intervals of 10% of the peak value. Negative contours are shown as dashed lines and the zero-level contour is shown by the bold line. (a) Natural weighting, all points weighted equally. (b) The points weighted so as to produce a uniform transfer function. (c) Heavily tapered weighting giving a wide beam. The use of the different weighting functions affects the beam width and the sidelobes because of the edge-diffraction pattern of the finite  $(u-v)$  coverage. The grating sidelobe response [due to the radical periodicity of the  $(u-v)$  coverage] and the coherent, near-in sidelobes [due to the gap in the  $(u-v)$  coverage] are unaffected by the different grading functions.

minimized. This is shown in Figure 10.8(c), where the outer spacings have been reduced by weighting. However, sidelobes caused by gaps in the  $(u,v)$  coverage (or feed support shadowing for a filled aperture) are not significantly effected by beam-weighting.

### c) Grating Responses

The discreteness of the interferometric data manifests grating responses which have no filled-aperture analogue. Many arrays are built with a regular spacing between the elements. This is often called a stepping interval for a variable spacing interferometer (Figure 10.7). The regular stepping interval  $D$  causes large responses at angles of  $n\lambda/D$  from the beam center, where  $n$  is a positive integer. These grating responses contain the same energy as in the central synthesized beam and they cannot be reduced by beam-weighting. For arrays which sample the  $(u,v)$  plane in two dimensions (Figure 10.7) the grating energy is distributed in an approximate ellipse, with an intensity peak of only  $\sim 10\%$  for the first ring. The grating responses of the one-dimensional arrays, as in Figure 10.6, are approximately equal to the main response. The stepping interval can be made smaller than an antenna radius, thus moving the response outside of the antenna primary beam,  $A(\sigma)$ . Some of the closer spacings less than the element diameter cannot be measured, and this leads to curvature in the zero level of the synthesized map.

### d) Bandwidth Correlation Area

Large-frequency bandwidths are often used for continuum measurements in order to increase the signal-to-noise ratio, which varies as the square root of the bandwidth. There are practical difficulties in using very wide bandwidths, however, since the characteristics of the RF, IF, and delay systems must be sufficiently frequency independent over the frequency range of interest.

Large bandwidths are also used to limit the coherence area of a synthesis array. Generally, a variable delay,  $\tau_D$ , is inserted in the IF line in order to compensate for the time-variable geometric delay,  $\tau(t)$ , such that the delay error,  $\Delta\tau = \tau_D - \tau(t)$ , is less than

the reciprocal bandwidth (see Section 10.2.2.b). However, the geometric delay varies with position in the sky, and for large interferometer spacings the change of the instantaneous geometric delay across the reception area of the array (generally, the primary beam area of the individual elements) is larger than the reciprocal bandwidth. Thus, if delay is inserted to equalize the geometric delay at the center of the reception area, radiation off-axis will not add coherently over the entire frequency bandwidth. In this way the correlation area of the array can be made smaller than the primary response area. Low-frequency arrays often use large bandwidths to limit the effective reception area (Moseley *et al.*, 1970; Erickson and Fisher, 1973).

The details of the bandwidth correlation area can be illustrated in the following manner. The calculation of  $\mathbf{b}$  for the synthesized beam or brightness distribution, given in Equations (10.29) and (10.30), has been implicitly determined using  $\omega_0$ , the center frequency of the RF bandpass. At another frequency  $\omega$  within the passband, the associated map will appear exactly the same except for the addition of a radial scale factor ( $\omega_0/\omega$ ) applied to the map coordinates. The integration over bandwidth  $\beta(\omega)$  will produce a radially smeared brightness distribution

$$I_{\beta}(\sigma) = \int \beta(\omega) I\left(\frac{\omega_0}{\omega}\sigma\right) d\omega \quad (10.31)$$

Thus, the result of an observation of a point source at the edge of the primary beam using a wide-band long-spacing array is a source extended in the radial direction at about the same centroid position. The total flux density of the source is unchanged but the peak brightness is lowered. In this way the response of the array to emission outside the primary beam area is rejected.

### e) Other Effects

A detailed analysis of many perturbations affecting a synthesized map have been considered by Brouw (1971) and will only be listed here.

- (1) The exact expansion of Equation (10.9) leads to an additional term to those in

Equations (10.13) and (10.14). Only for an east-west interferometer can the term be easily incorporated. The term is important for arrays larger than a few kilometers.

- (2) Errors in the synthesized pattern are caused by a phase offset, a phase variation, a baseline error or a gain variation, delay stepping, frequency dependence of the system, and time-constant effects.

### 10.3.3 Sensitivity

#### a) Random Noise

The sensitivity of a radio-telescope is usually discussed in terms of the random noise fluctuations due to contributions from the sky brightness, ground radiation, and receivers. Other causes of nonrandom noise—variously described as instabilities, atmospheric attenuation, scintillation, and interference—that limit the performance of a telescope or an array are discussed later.

A radio-telescope attempts to measure the noise power received from a radio source in the presence of a much larger power from the receivers themselves. What is important is not the large power of the unwanted noise signal but rather the statistical fluctuations in that power. If we integrate noise power in a bandwidth  $\Delta\nu$  Hz for a time  $t$  seconds, we have collected  $\Delta\nu t$  independent samples of the noise power. Statistical theory shows that the r.m.s. error in the estimate of the noise power is proportional to  $(\Delta\nu t)^{-1/2}$ . The noise fluctuations can be expressed in units of temperature,

$$\Delta T_{\text{r.m.s.}} = M \frac{T_s}{\sqrt{\Delta\nu t}} \quad (10.32)$$

where  $T_s$  is the system temperature and  $M$  is a factor ( $M \geq 1$ ) which depends on the method of observing. The system temperature includes contributions from receiver noise (which is usually dominant at frequencies larger than 100 MHz), sky brightness, and ground radiation entering the telescope feed and losses in the feed itself. A complete description of the calculation of the system tem-

perature is given by Christiansen and Högbom (1969).

In terms of a telescope with a geometric area  $Ag$  and efficiency  $\eta$  (typically  $\approx 0.5$ ), the flux density ( $\text{W m}^{-2} \text{ Hz}^{-1}$ ) r.m.s. fluctuation  $\Delta S_{\text{r.m.s.}}$  may be written as

$$\Delta S_{\text{r.m.s.}} = M \frac{2kT_s}{\sqrt{\Delta\nu t}} \frac{1}{\eta Ag} \quad (10.33)$$

where  $k$  = Boltzmann's constant =  $1.38 \times 10^{-23} \text{ W Hz}^{-1} \text{ K}^{-1}$ . An extra factor of 2 arises with unpolarized radiation, because only one-half of the power is intercepted by a feed.

The term "sensitivity" for an array has two interpretations, depending on the nature of the experiment performed. For unresolved sources the quantity of interest in the r.m.s. flux density fluctuation  $\Delta S_{\text{r.m.s.}}$  given by

$$\Delta S_{\text{r.m.s.}} = \sqrt{2} \frac{2kT_s}{\sqrt{\Delta\nu t}} \frac{1}{\eta Ai} \frac{1}{\sqrt{C}} \quad (10.34)$$

which can be derived directly from Equation (10.33), with the following considerations:

- (1)  $M = \sqrt{2}$  for a correlation receiver.
- (2)  $Ai$  = geometric aperture for an interferometer =  $2(Ag_1 \cdot Ag_2)^{1/2}$ , where  $Ag_{1,2}$  is the geometric aperture for each element. For identical elements  $Ai = 2Ag$  = total geometric area of the interferometer.
- (3)  $C$  = number of correlators. The maximum number of correlators is  $N(N - 1)/2$  for  $N$  elements.

For an array with many identical elements the r.m.s. noise fluctuation is equal to that of a single aperture (with an ideal receiver  $M = 1$ ) with a geometric area equal to that of the array. For calculating the minimum detectable flux density of a point source, the array configuration is inconsequential.

For extended sources of radio emission the r.m.s. noise of the brightness distribution  $\Delta I_{\text{r.m.s.}}$  is a useful parameter. The quantity is equal to that obtained by blurring  $S_{\text{r.m.s.}}$  over the synthesized beam.

$$\Delta I_{\text{r.m.s.}} = \frac{\Delta S_{\text{r.m.s.}}}{\Omega_{\text{syn}}} \quad (10.35)$$

where  $\Omega_{\text{syn}}$  is the equivalent solid angle of the synthesized beam. The brightness distribution of extended sources is commonly given in terms of brightness temperature  $T_b = (\lambda^2/2k) I$ . Thus

$$\Delta T_{br.m.s.} = \sqrt{2} \frac{T_s}{\sqrt{\Delta vt}} \frac{1}{\eta A_i} \frac{1}{\sqrt{C}} \frac{\lambda^2}{\Omega_{\text{syn}}} \quad (10.36)$$

The brightness sensitivity *decreases* with *increasing* resolution of an array, and the sensitivity to extended sources correspondingly becomes less.

All of the sensitivity parameters have been given in terms of a root-mean-square value. The correct use of a sensitivity depends on the nature of the experiment and the characteristic of the fluctuations causing the sensitivity limit. A detection limit of five times the r.m.s. fluctuation is commonly used.

Equations (10.34) to (10.36) give a lower bound to the sensitivities, since the assumption has been made that all observations of a given signal-to-noise are given equal weight (*i.e.*, natural weighting). In general, the efficiency  $E$  of the array is equal to

$$E = \frac{\sum_{i=1}^N w_i}{\left(N \sum_{i=1}^N w_i^2\right)^{1/2}} \quad (10.37)$$

where  $w_i$  is the additional weight above natural weighting of the  $i$ th point. If  $w_i = 1$  for all  $i$ ,  $E = 1$ ; otherwise  $E < 1.0$ .

An important result is the reduction of  $\Delta I_{r.m.s.}$  or  $\Delta T_{br.m.s.}$  by heavily tapering (weighting more heavily) the smaller spacings. Practical arrays undersample the longer baselines, and consequently further weighting the shorter spacings while decreasing the efficiency will nevertheless increase the sensitivity to an extended source. As an example, consider the set of observations shown in Figure 10.7. By disregarding data outside a radius  $R$  in the  $(u,v)$  plane, the synthesized beam area varies as  $R^{-2}$  but the efficiency  $E \sim R^{1/2}$ . Thus  $\Delta I_{r.m.s.} \propto \Delta T_{r.m.s.} \propto R^{-3/2}$ . For an extended source, optimal signal-to-noise will be achieved when the taper is such to produce a beam which matches in size the smallest

detectable source structure. For a point source, however, the peak brightness increases with resolution as  $R^2$ ; hence the net signal-to-noise is proportional to  $R^{1/2}$ , the efficiency.

A limitation to useful sensitivity in many telescopes is confusion rather than noise. With present-day techniques a sensitivity limit of  $10^{-29} \text{ W Hz}^{-1} \text{ m}^{-2}$  is obtainable. The density of sources is such that at frequencies less than 5000 MHz there are many sources above  $\Delta S_{r.m.s.}$  in the primary beam of even the largest filled apertures. These weak sources produce fluctuations larger than  $\Delta S_{r.m.s.}$  in the response of the telescope as it is moved. A useable sensitivity of  $\Delta S_{r.m.s.}$  can be reached only with better resolution, *i.e.*, with an extended array.

## b) Nonrandom Noise

### i) Interference

One has achieved a great deal if observations are limited by the random noise fluctuations described above. Radio astronomy has certain protected bands in which communications broadcasts are not permitted, but man-made interference is an ever-present threat. The legal limits on the ignition system of a London taxi are insufficient to prevent interference at a distance of 20 miles. For this reason radio observatories tend to be located in remote locations and partially protected by mountain ranges. The continuous increase in communications, radar, and satellites makes the threat to radio astronomy very real.

Arrays have an intrinsic rejection against interference, in that the unwanted signal must correlate in the proper phase and delay between the elements to produce interference.

### ii) Instabilities

Radio astronomy receivers have very high gains and small changes are amplified. Jumps in phase can occur due to a poor contact warming up, and slow drifts are not uncommon. Many of these instabilities can be calibrated out of the observations but often not perfectly.

## iii) Atmosphere

At longer wavelengths interplanetary clouds of electrons produce scintillations of small-angular-diameter sources. This phenomenon is valuable for measuring the approximate angular size of sources. Ionospheric variations produce large distortions of signals at meter and decimeter wavelengths, as anyone who listens to shortwave radio broadcasts well knows. At centimeter and millimeter wavelengths water vapor variations can produce variations in path length, causing large fluctuations in the phase in an interferometer. The effect of these variations causes higher sidelobe levels (Hinder and Ryle, 1971).

## 10.4 Inversion Techniques

## 10.4.1 Normal Inversion Methods

## a) Direct Inversion

The basic inversion equations have already been given in Section 10.1 (Equations 10.13 and 10.14). Expressed in the form of discrete observations, we get

$$I(x,y) = \sum_{k=1}^K w_k V(u_k, v_k) \exp \{ -i2\pi(u_k x + v_k y) \} \quad (10.38)$$

where  $V(u_k, v_k)$  is the visibility function of the  $k$ th point with projected spacing  $(u_k, v_k)$ ,  $(x, y)$  the sky coordinate, and  $w_k$  a weighting factor associated with each measured visibility function. The corresponding synthesized beam is given by

$$P(x,y) = \sum_{k=1}^K w_k \exp \{ -i2\pi(u_k x + v_k y) \} \quad (10.39)$$

the response to a point source. Each observation corresponds to average values of the visibility function and  $(u, v)$  coordinates over a certain restricted interval discussed in Section 10.3.1. The beam shape can be adjusted through the weighting parameters  $w_k$ , and the effect of the various weighting on the sensitivity, beam size, and sidelobe levels was discussed in Section 10.3.2.a.

For about 2500 input  $(u, v)$  points and a  $50 \times 50$  output  $(x, y)$  array (a modest amount of data), the computing time on a medium-sized computer is  $\sim 20$  minutes of execution time. The total number of steps requires  $\approx n^2 K \approx n^4$  basic operations where  $n \times n$  is the size of the  $(x, y)$  array and  $K$  is the number of sampled points. Clearly, for a large number of points, faster techniques must be resorted to.

## b) Fast Fourier Techniques

If the  $K$  input data points are interpolated into a rectangular  $(L \times M)$  array, the inversion in Equations (10.38) and (10.39) may be computed in the  $u$  and  $v$  coordinates separately, saving computing time.

$$I(x,y) = \sum_{l=1}^L \exp \{ -i2\pi u_l x \} \times \sum_{m=1}^M V'(u_l, v_m) \exp \{ -i2\pi v_m y \} \quad (10.40)$$

where  $(u_l, v_m)$  are the grid points and  $V'$  is the interpolated value of  $V$  (weighting included in  $V'$ ). The number of calculation steps  $\approx n^2 (M + L) \approx 2n^3$ , which is less than for the direct inversion.

For interferometric data obtained with a linear array, the Fourier inversion can also be computed in polar coordinates, with the radial and azimuthal sums separately calculated. In this case no interpolation is necessary.

Finally, by using a fast Fourier transform algorithm developed by Cooley and Tukey (1965), the number of computational steps may be reduced to  $\sim 2n^2 \log_2 n$ . Both the  $(x, y)$  and  $(u, v)$  planes are gridded as follows:

$$\begin{aligned} u_l &= l \times \Delta u & l &= -n \leq l \leq n-1 \\ v_m &= m \times \Delta v & m &= -n \leq m \leq n-1 \\ x_j &= j/2n\Delta u & j &= -n \leq j \leq n-1 \\ y_k &= k/2n\Delta v & k &= -n \leq k \leq n-1 \end{aligned}$$

then

$$I_{j,k} = \sum_{l=-n}^{-1} \sum_{m=-n}^{n-1} V'_{lm} \exp \left\{ -i\pi \frac{jl + km}{n} \right\} \quad (10.41)$$

where  $(\Delta u, \Delta v)$  are the increments in the  $(u, v)$  plane and  $(1/2n\Delta u, 1/2n\Delta v)$  are the corresponding increments in the  $(x, y)$  plane. The area in the sky of  $(1/\Delta u) \times (1/\Delta v)$  is called the "field of view."

The fast Fourier transform is a method used to conveniently compute the discrete Fourier transform of Equation (10.41). A readable description of the technique has been given in Cochran *et al.* (1967) and is not discussed in detail here. It is shown that the Fourier transform of  $N$  samples can be reduced to a simple sum of the Fourier transform of two samples, each with  $N/2$  samples with a saving of computing time. This reduction may be continued as long as the number of samples is divisible by 2. Thus, in a sample of  $N = 2^m$  points the original Fourier transform can be completely reduced to a number of computational steps much smaller than a straightforward application of Equation (10.41).

c) Gridding

The gridding of the data required by the fast Fourier transform involves two operations in the data. First, a convolution of the data is necessary to define the visibility function at the grid points. If  $c(u, v)$  is this convolution function, then

$$V'(u, v) = \int du' dv' V(u', v') c(u - u', v - v') \tag{10.42}$$

and

$$I'(x, y) = I(x, y) C(x, y) \tag{10.43}$$

where  $I(x, y)$  is the actual brightness distribution, and  $I'(x, y)$  is the brightness distribution after interpolation. The functions  $C(x, y)$  and  $c(u, v)$  are Fourier transform pairs.

Secondly, the sampling of the data at intervals  $\Delta u, \Delta v$  causes aliasing in the map. That is, the gridded distribution  $I''$  is given by

$$I''(x, y) = \sum_{M=-\infty}^{\infty} \sum_{N=-\infty}^{\infty} I' \left( x + \frac{N}{\Delta u}, y + \frac{M}{\Delta v} \right) \tag{10.44}$$

$$|x| < \frac{1}{\Delta u}, |y| < \frac{1}{\Delta v}$$

Thus, emission outside of the field of view will be reflected within the field of view. The primary response of the system and the factor  $C(x, y)$  will both decrease the response of the aliases.

The aliasing due to gridding and the grating lobes of a map are both due to a stepping interval in the data. The grating lobes depend on the measurement of the data and cannot be substantially changed. The aliasing is an artifact of the fast Fourier technique and is not inherent to the map. With proper gridding the increase of inversion speed far outweighs the complications due to gridding.

The simplest type of gridding is to average the visibility data into  $(u, v)$  cells of size  $\Delta u \times \Delta v$ , with the summed visibility function becoming  $V'(u, v)$ . The convolving function in this case is  $c(u, v)$ , where  $c(u, v) = 1$  for  $|u| < \Delta u/2$  and  $|v| < \Delta v/2$ ;  $c(u, v) = 0$  otherwise. The convolution in the  $(u, v)$  plane tapers the brightness distribution by\*

$$\frac{\sin(\pi\Delta ux)}{\pi\Delta ux} \times \frac{\sin(\pi\Delta vy)}{\pi\Delta vy}$$

If the  $V'(u, v)$  is then sampled with interval  $\Delta u \times \Delta v$ , aliasing occurs, as defined by Equation (10.44). Although attenuated by the  $|\sin x/x|$  terms, the aliasing can be very annoying in complicated brightness distributions. A simple solution is to enlarge the field of view and to significantly reduce the aliasing from adjacent images of the sky plane. The visibility function can also be convolved with a Gaussian function. This leads to a more desirable tapering of the brightness distribution than a simple averaging into cells, but is more time-consuming in a computer.

The choice of gridding also depends upon the type of observation. If a bright small-diameter source of extent  $\Delta x$  by  $\Delta y$  is synthesized, a grid size of  $\Delta u \sim (1/\Delta x)$ ,  $\Delta v \sim (1/\Delta y)$  (Bracewell, 1958) is acceptable. The aliasing of weak emission outside of the source

\* A predictable relationship between the convolving and tapering functions exists only when the cells contain many data points randomly situated in the cell.

area is insignificant. At the other extreme, there is no need to grid more finely than about a half-diameter of the antenna size. The aliases are then well outside of the primary beam response and the grating response.

#### d) Analogue Methods

Apart from the above digital inversion techniques, which are the ones that have been used in practice, there exist in principle a number of analogue procedures based on the Fourier transform relationship in other realms of physics. For example, the diffraction pattern formed by an aperture illuminated by monochromatic light is the Fourier transform of the distribution of brightness across the aperture.

If this aperture were an analogue image of the  $(u,v)$  plane (say a photographic emulsion giving both amplitude and phase changes to the wavefront), then the diffraction pattern would be an image of the sky brightness distribution. Some of these analogue techniques have already been put into practice in speckle interferometry of starlight.

#### 10.4.2 Other Inversion Methods

The Fourier inversion process discussed above typically leads to sidelobe levels of about 5%, even with good interferometric coverage in the  $(u,v)$  plane. Thus, faint features which are still more intense than the noise fluctuations can be obscured by the sidelobes of strong features. With incomplete  $(u,v)$  coverage, such as is obtained with a non-east-west line array, with sidelobe levels of perhaps 30%, the problem of recognizing low-intensity regions is even more difficult. Finally, interferometric data with inaccurate or undetermined phase information cannot be inverted using a Fourier analysis and other methods must be considered.

Many schemes have been developed which determine the brightness distribution from a given set of visibility functions. Most of the methods are not amenable to complete analysis because of their nonlinear character,

so derivations of uniqueness of solution or the errors of solution are difficult to ascertain. The schemes fall into two subclasses: model-fitting methods which use the measured visibility function directly to determine a compatible brightness distribution; and methods that use a Fourier inversion to obtain the brightness distribution which is then improved using the characteristics of the synthesized beam or some other criteria.

#### a) Model Fitting

Model fitting is an attempt to reproduce the observed visibility function using a simple brightness distribution which is composed of a collection of discrete components. The fitting procedure is usually an iterative one, in which the parameters describing the model (*i.e.*, number of components, specific values for component parameters) are adjusted until a satisfactory fit is obtained between the observed visibility function and the model visibility function (Fomalont, 1968). This type of analysis is one which minimizes an error difference,  $\Delta V_i$ , by adjusting a model described by a set of parameters,  $P_i$ , such as

$$\Delta V_i = \sum_{k=1}^K w_k |V(u_k, v_k) - M(u_k, v_k; P_i)|^2 \quad (10.45)$$

The summation is over the  $K$  measurement of the visibility function  $V$ . The weight of each point is  $w_k$ , and  $M(u_k, v_k; P_i)$  is the model visibility function with a set of input parameters  $P_i$ . Gaussian-shaped components are most commonly used because of their convenient Fourier transform. In specific cases, other component shapes can be used. A uniformly illuminated circular disk, for example, is often used in analyzing high-resolution observations of planetary surfaces. Sample visibility functions for model sources are shown in the Appendix III.

Model fitting is most useful in analyzing interferometric data of strong, isolated small-diameter sources. For such data, which are completely defined by a small number of parameters (flux density, position and diameter of each component), a model-fitting

technique satisfactorily determines accurate parameter values. The values may be difficult to obtain directly from a Fourier inversion because of the complication of the beam shape and sidelobes. Model fitting can be used for inverting complicated brightness distributions, but this requires a good method for minimizing  $\Delta V$  and also leads to excessive computation time for a large amount of data.

Model fitting is a useful method for inverting data having very poor or no phase information. The error  $\Delta V$  in Equation (10.45) can be defined in terms of the visibility amplitude instead of the visibility function, but the analysis technique is the same. For data with no phase information the position of the brightness distribution and its axial symmetry is arbitrary.

The solution of Equation (10.45) cannot be described in detail here. A least-square analysis usually leads to a nonlinear set of normal equations determined by  $\partial V_i / \partial P_i$ . The equations can be linearized in the neighborhood of an initial guess solution and small changes of the model parameters can be obtained. The improved solution is then used as an initial guess for the next iteration, etc. Convergence is not assured and is very slow for a complicated model. A more useful method, called a simplex analysis, is described by Nielsen (1964, p. 336).

Bates (1969) has discussed the interpretation of interferometric data with little or no phase information. He describes the square of the modulus of the observed visibility function in terms of the position of its zeroes in the complex  $(u, v)$  plane. The zeroes form conjugate pairs, and a complex visibility function whose modulus is equal to that observed can be generated by arbitrarily choosing one zero from each pair. If the modulus is defined by  $N$  zero pairs, then there are  $2^N$  possible visibility functions. However, many of these solutions are not satisfactory because of significant negative response over part of the brightness distribution. The use of some phase information can further limit the acceptable choice of zero pairs.

### b) Source Subtraction

Often maps of radio sources contain obvious sidelobe structure from several intense features in the field or other strong sources within the primary response and delay pattern. These sidelobes distort and hide weak and underlying structures, and it is difficult to disentangle by eye the real from the spurious features. A useful method of removing these sidelobes is to subtract the corresponding visibility function of the intense feature from the total visibility function. The inversion of the remainder will then be a map with the intense feature and all of its sidelobe removed. This process can be repeated as long as there are intense components which dominate the map. It is not necessary that the removed sources be within the field of view if a gridded inversion scheme is used after the subtraction.

The parameters of the source to be subtracted from the map should be precisely determined in order to remove completely the associated sidelobes. This can be done from measurements from the inverted map; however, the model-fitting technique described above can be used to better estimate exact parameters for the intense features. This is especially true if the intense features are somewhat larger than the synthesized beam.

The combination of source subtraction and model fitting is useful for incomplete aperture synthesis of relatively simple sources. Although the original map may contain sidelobe levels of 30%, after the subtraction of a reasonable model fit solution, the resulting sidelobe level of the remaining structure may be at only a 5% level of the original scale.

### c) Cleaning

A useful method, called cleaning, corrects a map for the presence of sidelobes (Högbom, 1973). Cleaning is a type of band-limited deconvolution in which the brightness distribution is decomposed into a sum of beam patterns. Let  $I_D(x, y)$  be the brightness distribution found by the inversion (dirty map) and  $P_D(x, y)$  the corresponding beam (dirty

beam). We wish to determine the set of numbers  $A_i(x_i, y_i)$  such that

$$I_D(x, y) = \sum_i A_i P_D(x - x_i, y - y_i) + I_R(x, y) \quad (10.46)$$

where  $I_R(x, y)$  is the residual brightness distribution after the decomposition. Normally, the decomposition is made from a gridded high-speed inversion for faster computing. The solution is considered satisfactory if  $I_R(x, y)$  is of the order of the expected noise.

An important feature of cleaning is the ease with which the constraint of source size can be incorporated in the analysis. The field of search in the  $(x, y)$  plane can be arbitrarily limited to any region(s) by determining the values of  $A_i$  only in the region of the expected emission. If the region has been properly chosen,  $I_R(x, y)$  should be small over the entire field of view. If there is emission outside the cleaning region, it will still appear in the residual term. Unlike source subtraction in the visibility plane, the region searched for sources must be well within the field of view if gridded inversion schemes are used.

The decomposition of Equation (10.46) cannot be done analytically. An iterative technique commonly used is:

- (1) Determine dirty map,  $I_D(x, y)$ , and dirty beam,  $P_D(x, y)$ , using the same inversion methods.
- (2) Find maximum value in the search area of  $|I_D(x, y)|$ ; denoted by  $I_i$  at position  $(x_i, y_i)$ .
- (3) Subtract some fraction  $q$  of the dirty beam centered at  $(x_i, y_i)$  from the dirty map.

$$I_D'(x, y) = I_D(x, y) - q I_i P_D(x - x_i, y - y_i)$$

- (4) Go back to step (2) and operate on  $I_D'$ .
- (5) Terminate the iteration cycle when
  - (a)  $I_i$  is less than a specified value
  - (b) the number of iterations exceed a limit
  - (c)  $I_i$  stops decreasing or begins to increase.

The technique yields a set of beam patterns of amplitude  $I_i$  and position  $(x_i, y_i)$ , the sum of which approximately reproduces

the original brightness distribution. During the iteration cycle the subtraction of a dirty beam at any point may occur several times. In practice the value of  $q \approx 0.5$  gives fast and accurate convergence.

The cleaned map is obtained by the summation in Equation (10.46), with the dirty beam,  $P_D$ , being replaced by a clean beam,  $P_C$ . The clean beam is arbitrary but is most conveniently taken to be a Gaussian function with an elliptical beamwidth which matches that of the dirty beam.

Analysis of the cleaning procedure is difficult because of the iterative nature of the method. Practically the method works extremely well. If the cleaning area is well chosen, it is not uncommon to produce clean maps with no sidelobes above the noise level. Dirty maps with 30% sidelobe structures can be cleaned to a level of a few percent with adequate signal-to-noise. An example of cleaned maps is given in Figure 10.9. The corresponding dirty beam and dirty map are shown in Figure 10.8. Care must be taken in the inversion process so that the dirty map is, in fact, the convolution of the real brightness distribution and the dirty beam.

#### d) Maximum Entropy Analysis

A possible new method for determining the brightness distribution from a measured set of visibility functions has been developed by Burg (1973) for use in auto-correlation data; it has been generalized by Ables (1973) for interferometric data.

The usual inversion techniques (except for model fitting) implicitly assume a value of zero for the visibility function at unmeasured points in the  $(u, v)$  plane. This produces larger sidelobes and poorer resolution than necessary but, at least, defines a unique synthesized beam pattern—and improved maps can be obtained, as described in the previous section.

The maximum entropy analysis uses only those measured data and derives a brightness distribution which is the most random, *i.e.*, has the maximum entropy of any brightness distribution consistent with the measured data. The technique has been used success-

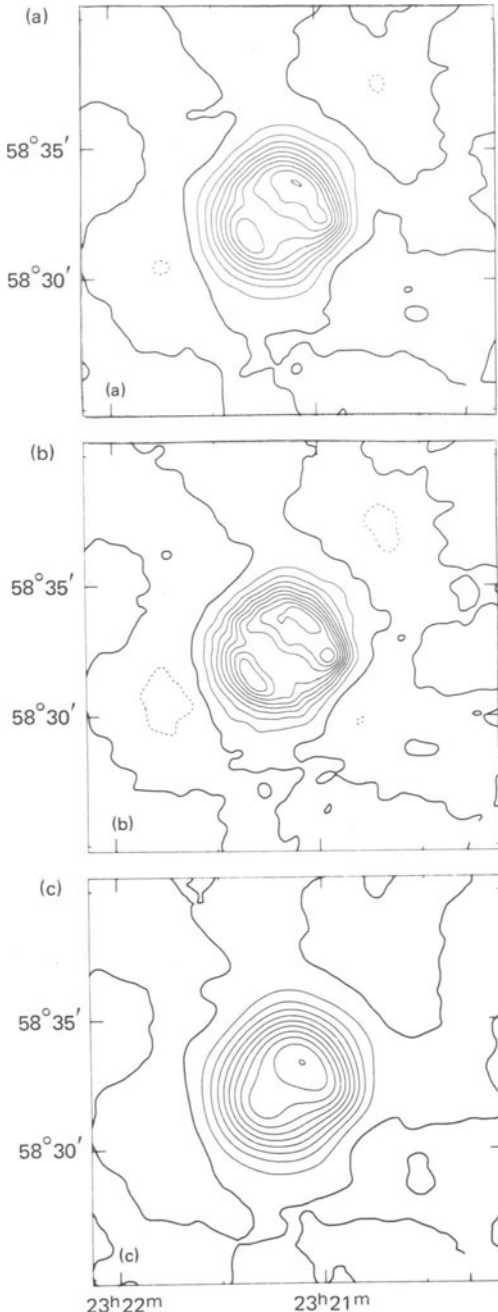


**Figure 10.9** The results of using the cleaning inversion technique on CAS A. The dirty beam and dirty map have been taken from that in Figure 10.8(b).

fully on gridded one-dimensional data with improved resolution, virtually no sidelobes, and little extra cost in computational time.

However, the generalization to two-dimensional data may involve an excessive amount of computer time.

## Appendix

### I. Interferometric Parameters

Various quantities associated with interferometers are shown in Figure 10.A1. Given a separation of two antennas in kilometers and an observing frequency, the separation in wavelengths, the minimum fringe size, the maximum fringe rate due to the diurnal motion, and the maximum delay of a signal between antennas can be found. Lines corresponding to the radio frequencies 30 MHz, 300 MHz, 3 GHz, and 30 GHz as well as a typical optical frequency are given.

The determination of accurate pulsar positions using the change of pulsar phase with the Earth orbital motion is an interferometric technique. The frequency of the signal is equal to the pulsar repetition rate and the interferometer baseline is equal to the diameter of the orbit of the Earth. Positional accuracy to about 1/100 of a fringe size is obtained.

### II. Fringe-Source Geometry

#### A) Baseline Coordinates

The equatorial coordinate system is generally used for describing the source and interferometer parameters. See Figure 10.A2.

$\hat{e}_x$  toward the point  $\delta = 0^\circ, h = 0^h$  } left-  
 $\hat{e}_y$  toward the point  $\delta = 0^\circ, h = 6^h$  } handed  
 $\hat{e}_z$  toward the point  $\delta = 90^\circ$  } system

(1) Baseline vector  $\mathbf{B}$  of length  $B$  (in any appropriate set of units) and direction defined from telescope 2 to telescope 1 with coordinates Declination  $D$  and hour angle  $H$  are given by

$$\begin{pmatrix} B_x \\ B_y \\ B_z \end{pmatrix} = \begin{pmatrix} B \cos D \cos H \\ B \cos D \sin H \\ B \sin D \end{pmatrix}$$

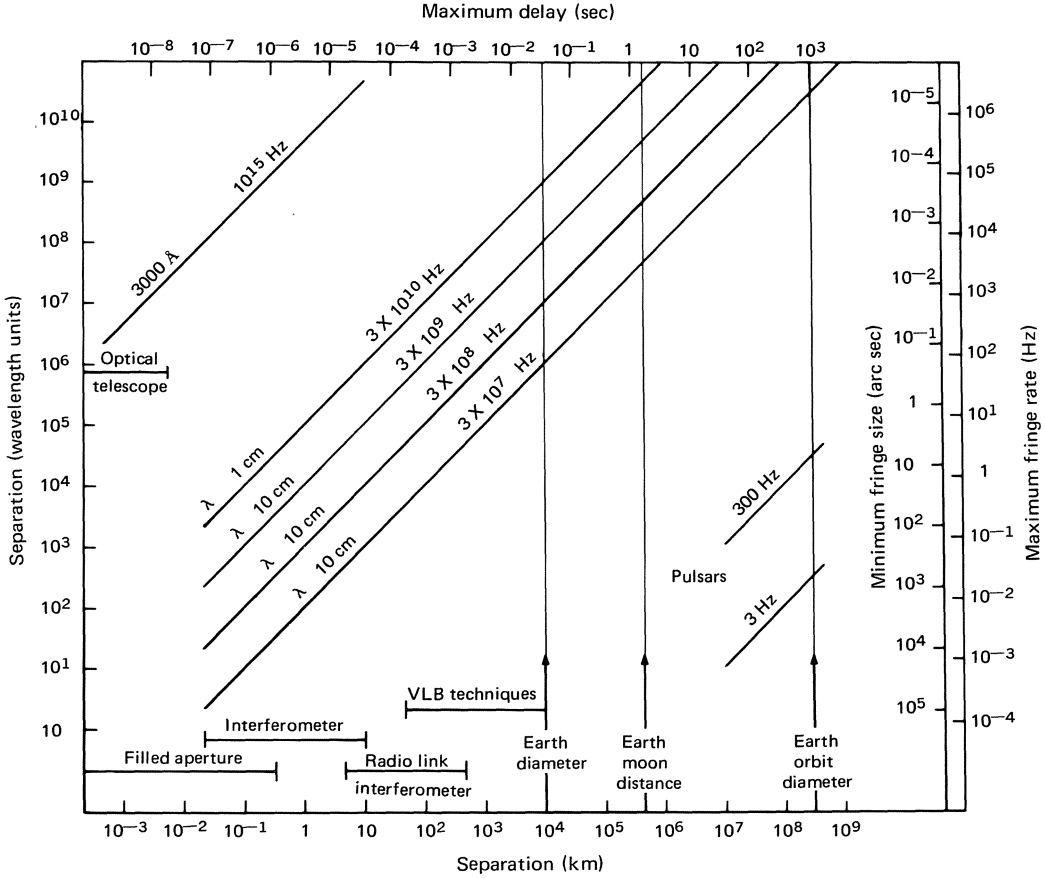


**Figure 10.A1** Interferometric parameters. Given the interferometer separation in kilometers and the observing frequency, the separation in wavelengths, the maximum delay, the maximum fringe rate, and the minimum fringe size can be obtained. The range of separation used for the most common techniques of interferometry is shown at the lower part of the diagram.

- (2) Source direction  $\mathbf{s}$  (unit vector) given by declination  $\delta$  and hour angle  $h$  is

$$\begin{pmatrix} s_x \\ s_y \\ s_z \end{pmatrix} = \begin{pmatrix} \cos \delta \cos h \\ \cos \delta \sin h \\ \sin \delta \end{pmatrix}$$

- (3) For an azimuthal description of the baseline  $\mathbf{B}$  in terms of  $B_{\text{north}}$  and  $B_{\text{east}}$  (the ground projections) and  $B_{\text{elev}}$  (the elevation difference),

$$\begin{pmatrix} B_x \\ B_y \\ B_z \end{pmatrix} = \begin{pmatrix} -\sin L & 0 & \cos L \\ 0 & -1 & 0 \\ \cos L & 0 & \sin L \end{pmatrix} \begin{pmatrix} B_{\text{north}} \\ B_{\text{east}} \\ B_{\text{elev}} \end{pmatrix}$$

where  $L$  is the latitude. This description is valid over only small distances, where the

effect of the Earth's curvature is negligible.

- (4) The delay is given by

$$\begin{aligned} \mathbf{B} \cdot \mathbf{s} &= B_x \cos \delta \cos h + B_y \cos \delta \sin h + B_z \sin \delta \\ &= B(\sin \delta \sin D + \cos \delta \cos D \cos(h - H)) \end{aligned}$$

in the same units as  $B$ .

- (5) The angle  $\theta$  between the interferometer pole and the source is

$$\begin{aligned} \cos \theta &= \frac{\mathbf{B} \cdot \mathbf{s}}{|\mathbf{B}|} = \sin \delta \sin D + \cos \delta \cos D \cos(h - H) \\ &= \cos(\delta - D) - \cos \delta \times \cos D (1 - \cos(h - H)) \end{aligned}$$

(6) The fringe frequency  $\nu_f$  in hertz is given by

$$\begin{aligned} \nu_f &= |\mathbf{B}| \cdot \frac{d(\cos \theta)}{dh} = -|\mathbf{B}| \cos \delta \cos D \\ &\quad \times \sin(h - H) \\ &= \cos \delta [B_y \cos h \\ &\quad - B_x \sin h] \end{aligned}$$

where  $B$  is in wavelengths.

B) Derived Quantities

The astrometric coordinate system is used for describing a tracking interferometer. See Figure 10.A2.

- $\hat{e}_u$  west to east as viewed from the source
- $\hat{e}_v$  south to north as viewed from the source
- $\hat{e}_w$  from source to observer.

(1) Baseline vector  $\mathbf{B}$  becomes

$$\begin{pmatrix} B_u \equiv u \\ B_v \equiv v \\ B_w \equiv \mathbf{B} \cdot \mathbf{s} \end{pmatrix}$$

$$= \begin{pmatrix} \sin h & -\cos h & 0 \\ -\sin \delta \cos h & -\sin \delta \sin h & \cos \delta \\ \cos \delta \cos h & \cos \delta \sin h & \sin \delta \end{pmatrix} \begin{pmatrix} B_x \\ B_y \\ B_z \end{pmatrix}$$

$\mathbf{b} = \hat{e}_u u + \hat{e}_v v$  is the projected spacing and  $B_w = \mathbf{B} \cdot \mathbf{s}$  is the delay.

(2) For a tracking interferometer the path of the projected baseline in the  $(u,v)$  plane over a 24-hour period is given by the ellipse

$$\frac{u^2}{a^2} + \frac{(v - v_o)^2}{b^2} = 1$$

where

$$a = \sqrt{B_x^2 + B_y^2} = B \cos D$$

$$b = a \sin \delta = B \cos D \sin \delta$$

$$v_o = B_z \cos \delta = B \sin D \cos \delta$$

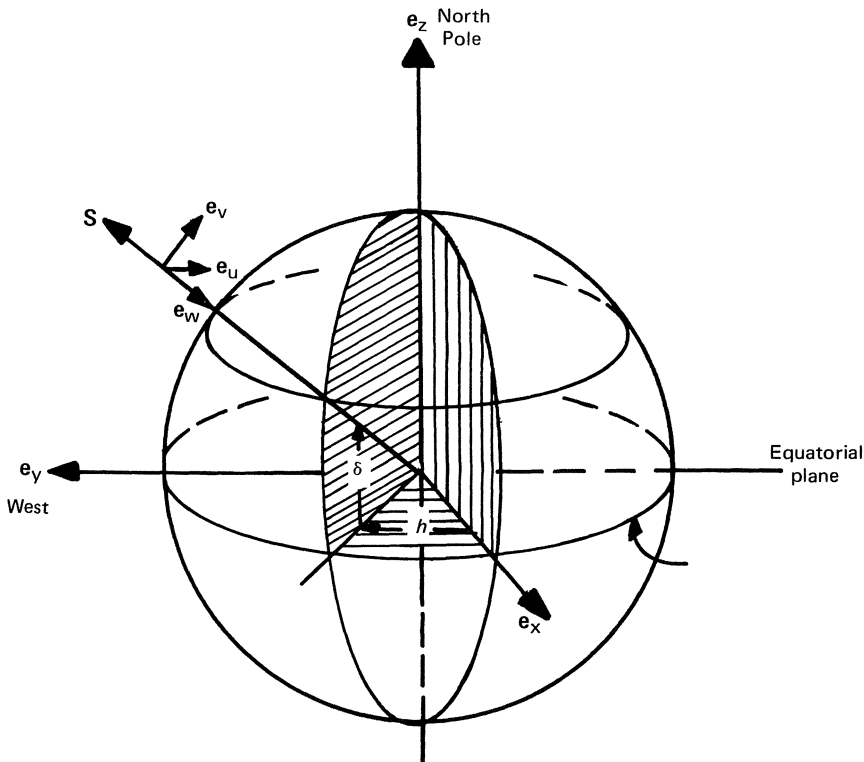
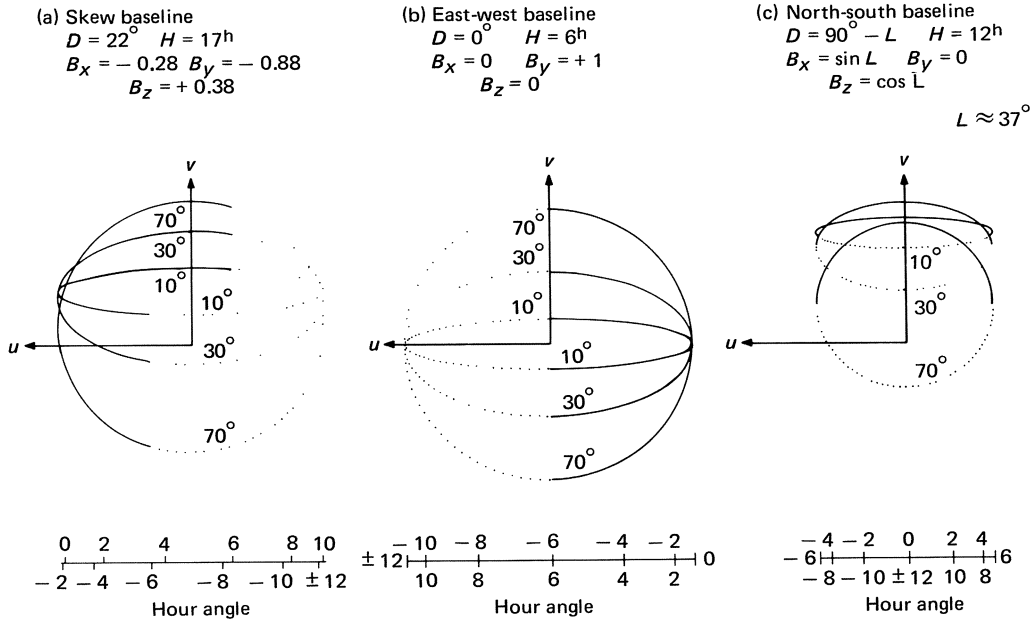


Figure 10.A2 Equatorial and astrometric coordinates used in interferometry. The unit vectors  $\hat{e}_x, \hat{e}_y, \hat{e}_z$  form the equatorial system. The unit vectors  $\hat{e}_u, \hat{e}_v, \hat{e}_w$  form the astrometric system. The direction of the source is given by  $\mathbf{s}$ .



**Figure 10.A3** The loci of points in the  $(u-v)$  plane produced by a tracking interferometer for: (a) a skew baseline, (b) an east-west baseline, (c) a north-south baseline. The loci are drawn for declinations  $70^\circ$ ,  $30^\circ$ , and  $10^\circ$ . The solid portion of each curve is given for the hour angle range  $-6^h$  to  $+6^h$ , the dotted portion for the hour angles  $+6^h$  to  $+18^h$ . The hour angle scale, which is a function only of  $u$ , is given at the bottom of each diagram. For declinations south of the equator, use the curve with positive declination but flip the curves around  $v = v_0$ .

Examples are given in Figure 10.A3.

- (3) The term  $\sigma$ , a displacement from the phase center direction  $\mathbf{s}$ , may be written as

$$\begin{pmatrix} \sigma_u \\ \sigma_v \\ \sigma_w \end{pmatrix} = \begin{pmatrix} \Delta\alpha \cos \delta \\ \Delta\delta \\ 0 \end{pmatrix}$$

Neglecting the sky curvature one obtains,

$$\mathbf{B} \cdot \boldsymbol{\sigma} = u\Delta\alpha \cos \delta + v\Delta\delta = \mathbf{b} \cdot \boldsymbol{\sigma}$$

### III. Visibility Functions Corresponding to Simple Brightness Models

The visibility function  $V(u,v)$  can be obtained from the brightness distribution  $I(x,y)$  using Equation (10.13):

$$V(u,v) = \int dx \int dy I(x,y) \exp \{i2\pi(ux + vy)\}$$

In Section 10.4 we discussed the general methods used to invert interferometric data. However, it is often useful to look at the general behavior of the visibility function in

order to determine the approximate brightness distribution, which may then be helpful in choosing correct inversion parameters. For this reason model visibility functions are given in Figure 10.A4. For simplicity the visibility functions are plotted for an east-west projected spacing, except for the last plot. The visibility functions for any position angle can then be easily obtained. The visibility function amplitude (normalized to unity at zero spacing) is shown by the solid line; the visibility function phase is given by the dashed line in units of lobes (revolutions). All of the models can be scaled.

Details of each model are:

- (a) The visibility function for a displaced point source. The displacement of the source along the angle of resolution produces a phase gradient. A displacement of 1 arc second gives a phase shift of 1 lobe at 206,265 wavelengths.

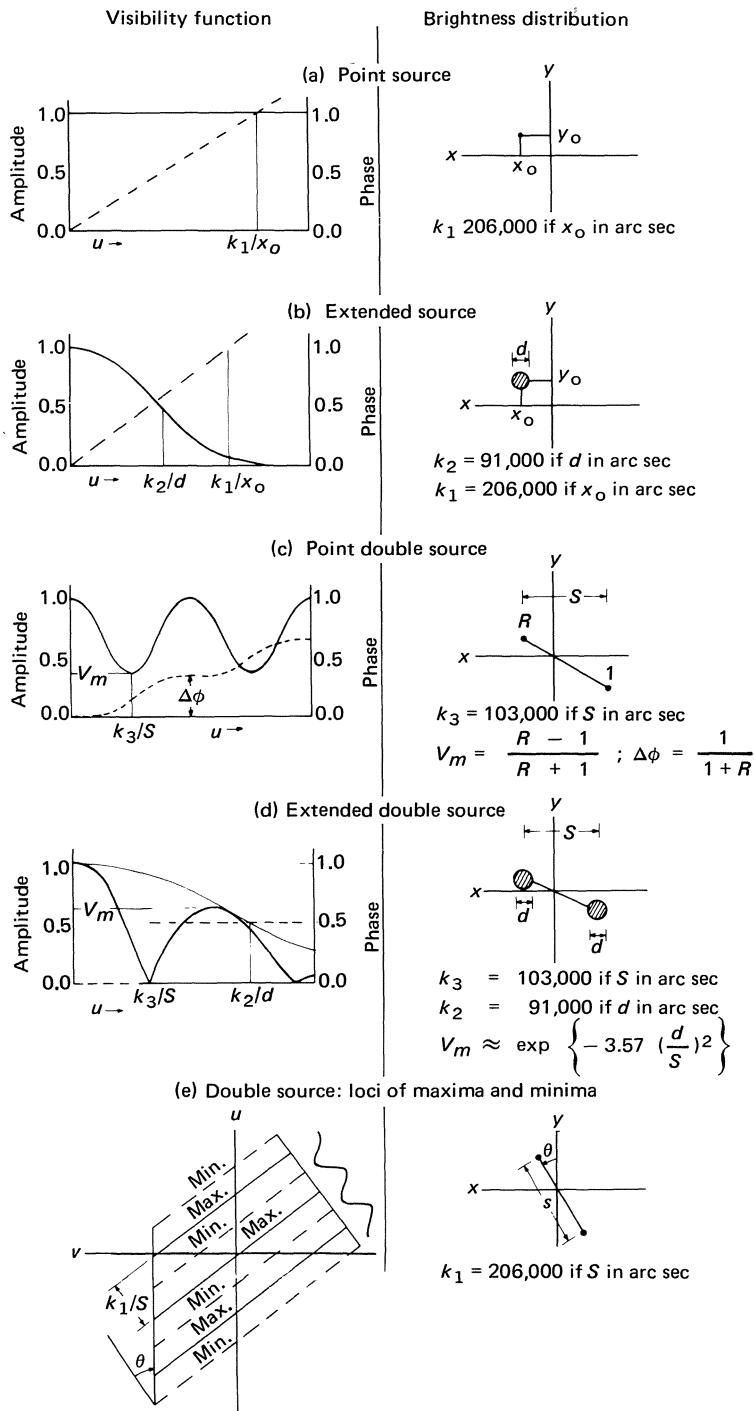


Figure 10.A4 The visibility functions for various brightness distribution models (see text).

- (b) The visibility function for a displaced Gaussian source. The phase behavior is identical to the point source. The visibility amplitude is also Gaussian. A source of diameter 1 arc second (half-power diameter) yields a visibility, with half-amplitude at 91,000 wavelengths.
- (c) The visibility function for a point double source. The minimum amplitude and the change of phase between successive maxima are both related to the intensity ratio,  $R$ , of the double. The period of the amplitude depends on the double separation. The sign of the phase change gives the direction of the stronger component, positive to east. The centroid of the double has been taken as the phase center.
- (d) The visibility function for an equal double. The model is similar to that of an equal point double, with the visibility amplitude multiplied by an envelope equal to the visibility amplitude of the individual component. The axial ratio,  $s/d$ , of the double is given by the amplitude of the first maximum.
- (e) The loci of visibility amplitude maxima and minima in the  $(u, v)$  plane for a double source. Lines of constant maxima are given by the solid lines, lines of constant minima by the dashed lines.

#### IV. Interferometric Polarimetry

##### A. General Expression

The output of a two-element interferometer given in Equation (10.11) can be generalized for arbitrary polarization and feed characteristics. If  $\phi$  is the orientation of the feed and  $\theta$  is the ellipticity, then the response function of the feed  $\mathbf{G}$  is

$$\mathbf{G} = \hat{\mathbf{e}}_x (\cos \theta \cos \phi - i \sin \theta \sin \phi) + \hat{\mathbf{e}}_y (\cos \theta \sin \phi + i \sin \theta \cos \phi) \quad (10.A4.1)$$

and the voltage response to the generally polarized beam of Equation (10.17) is the complex dot product  $\mathbf{G} \cdot \mathbf{E}$  for the polarized part of the radiation and  $(1/\sqrt{2}) |E_u|$  of the unpolarized part. If  $\mathbf{G}_1$  and  $\mathbf{G}_2$  are the

characteristics of the two feeds, then the interferometer response is sensitive to the part of the radiation given by

$$(\mathbf{G}_1 \cdot \mathbf{E}) \times (\mathbf{G}_2 \cdot \mathbf{E})^* + \frac{1}{2}(\mathbf{G}_1 \cdot \mathbf{G}_2) |E_u|^2 \quad (10.A4.2)$$

which can be written in terms of  $|Ex|^2$ ,  $|Ey|^2$ ,  $ExEy^*$ ,  $Ex^*Ey$ —the four polarization coherence functions. A more useful method is to write the response in terms of the four Stokes parameters,  $I$ ,  $Q$ ,  $U$ , and  $V$ .

From Equations (10.11), (10.17), (10.A4.1), and (10.A4.2) we get

$$R(t) = \exp \{i2\pi \mathbf{B} \cdot \mathbf{s}\} \int d\sigma F(\boldsymbol{\sigma}) \exp \{i2\pi \mathbf{b} \cdot \boldsymbol{\sigma}\} \quad (10.A4.3)$$

with

$$\begin{aligned} 2F(\boldsymbol{\sigma}) = & I(\boldsymbol{\sigma}) \{ \cos(\phi_1 - \phi_2) \cos(\theta_1 - \theta_2) \\ & - i \sin(\phi_1 - \phi_2) \sin(\theta_1 + \theta_2) \} \\ & + Q(\boldsymbol{\sigma}) \{ \cos(\phi_1 + \phi_2) \cos(\theta_1 + \theta_2) \\ & - i \sin(\phi_1 + \phi_2) \sin(\theta_1 - \theta_2) \} \\ & + U(\boldsymbol{\sigma}) \{ \sin(\phi_1 + \phi_2) \cos(\theta_1 + \theta_2) \\ & + i \cos(\phi_1 + \phi_2) \sin(\theta_1 - \theta_2) \} \\ & + V(\boldsymbol{\sigma}) \{ \cos(\phi_1 - \phi_2) \sin(\theta_1 + \theta_2) \\ & - i \sin(\phi_1 - \phi_2) \cos(\theta_1 - \theta_2) \} \end{aligned}$$

where

$(\theta_1, \phi_1)$  = ellipticity and orientation of feed 1

$(\theta_2, \phi_2)$  = ellipticity and orientation of feed 2

$\mathbf{B}$  = baseline (defined from antenna 2 to antenna 1)

$\mathbf{b}$  = projected spacing

$\mathbf{s}$  = position of phase center

$\boldsymbol{\sigma}$  = angular coordinate

$I = E_o^2 + E_u^2$  = total intensity

$$\begin{aligned} Q &= E_o^2 \cos 2\beta \cos 2\chi \\ U &= E_o^2 \cos 2\beta \sin 2\chi \end{aligned} = \begin{cases} E_o^2 \cos 2\beta \\ \times \exp(i2\chi) \\ = Q + iU \\ = P = \text{linear} \\ \text{polarization} \end{cases}$$

$V = E_o^2 \sin 2\beta$  = Circular polarization (left-hand positive)

B. Specific Examples

(a) Almost parallel feeds

$$\begin{aligned} \phi_2 &= \phi_1 - \Delta\phi & \theta_2 &= \theta_1 - \Delta\theta \\ F_{11}(\sigma) &= I(\sigma) + Q(\sigma) \cos 2\phi_1 \cos 2\theta_1 \\ &+ U(\sigma) \sin 2\phi_1 \cos 2\theta_1 \\ &+ V(\sigma) \sin 2\theta_1 - i I(\sigma) \Delta\phi \sin 2\theta_1 \\ &+ \text{smaller terms if } I \gg Q, U, V \end{aligned}$$

(b) Almost perpendicular feeds

$$\begin{aligned} \phi_2 &= \phi_1 + \frac{\pi}{2} - \Delta\phi & \theta_2 &= -\theta_1 - \Delta\theta \\ F_{11}(\sigma) &= Q(\sigma) [-\sin 2\phi_1 \\ &- i \cos 2\phi_1 \sin 2\theta_1] + U(\sigma) [\cos 2\phi_1 \\ &- i \sin 2\phi_1 \sin 2\theta_1] + V(\sigma) [i \cos 2\theta_1] \\ &+ I(\sigma) [\Delta\phi \cos 2\theta_1 - i\Delta\theta] \\ &+ \text{smaller terms if } I \gg Q, U, V \end{aligned}$$

(c) Linear polarized feeds

$\theta_1 = \theta_2 = 0$ , with the orientation designated by  $F_{\phi_1, \phi_2}(\sigma)$

$$\begin{aligned} F_{0,0}(\sigma) &= I(\sigma) + Q(\sigma) \\ F_{90,90}(\sigma) &= I(\sigma) - Q(\sigma) \\ F_{45,45}(\sigma) &= I(\sigma) + U(\sigma) \\ F_{135,135}(\sigma) &= I(\sigma) - U(\sigma) \\ F_{0,90}(\sigma) &= U(\sigma) + iV(\sigma) \\ F_{45,135}(\sigma) &= -Q(\sigma) + iV(\sigma) \\ F_{90,0}(\sigma) &= -F_{90,180}(\sigma) = U(\sigma) - iV(\sigma) \\ F_{135,45}(\sigma) &= -F_{135,225}(\sigma) \\ &= -Q(\sigma) - iV(\sigma) \end{aligned}$$

(d) Circularly polarized feeds

$$\begin{aligned} \phi_1 + \phi_2 &= \phi: & \text{arbitrary} \\ \theta &= \pi/4 \text{ (left hand = } L), \theta = -\pi/4 \text{ (right} \\ & & \text{hand = } R) \\ F_{LL}(\sigma) &= [I(\sigma) + V(\sigma)] \exp(-i2\phi) \\ F_{RR}(\sigma) &= [I(\sigma) - V(\sigma)] \exp(-i2\phi) \\ F_{LR}(\sigma) &= [Q(\sigma) + iU(\sigma)] \exp\{-i2\phi\} \\ F_{RL}(\sigma) &= [Q(\sigma) - iU(\sigma)] \exp\{-i2\phi\} \end{aligned}$$

V. Bandwidth and Fringe-Washing Functions

(a) The monochromatic response at frequency  $\omega$  is (see Figure 10.4)

$$\begin{aligned} R_\omega(t) &= \cos \{ \omega [(\tau(t) - \tau_D] \\ & \quad + \omega_o \tau(t) - \phi(t) \} \\ &= \text{Real} \{ \exp [i\omega(\tau(t) - \tau_D)] \\ & \quad \times \exp [i\omega_o \tau(t) - i\phi(t)] \} \end{aligned}$$

(b) The broad-band response is

$$R(t) = \int \alpha(\omega) R_\omega(t) d\omega$$

where  $\alpha(\omega)$  is the bandpass of the system. This can be written as

$$R(t) = \exp [i\omega_o \tau(t) - \phi(t)] \int \alpha(\omega) \exp\{i\omega \Delta\tau\} d\omega$$

and using  $\Delta\tau \equiv \tau(t) - \tau_D =$  delay offset becomes

$$R(t) = \beta(\Delta\tau) \exp i\{\omega_o \tau(t) - \theta(t)\}$$

where

$$\beta(\Delta\tau) \equiv \int \alpha(\omega) \exp\{i\omega \Delta\tau\} d\omega$$

is the fringe-washing function.

Examples of  $\alpha(\omega) - \beta(\Delta\tau)$  pairs are given by Christiansen and Högbom (1969).

References

Ables, J. 1974. Submitted to *Astron. Astrophys.*, in press.  
 Baldwin, J. E., C. J. Field, P. J. Warner, and M. C. H. Wright. 1971. *Monthly Notices Roy. Astron. Soc.* 154:445.  
 Basart, J. P., G. K. Miley, and B. G. Clark. 1970. *IEEE Trans., Ap-18*, 375.  
 Bates, R. H. T. 1969. *Monthly Notices Roy. Astron. Soc.* 142:413.  
 Bracewell, R. N. 1958. *Proc. IRE* 46:97.  
 Brouw, W. N. 1971. Doctoral dissertation. Leiden University.  
 Burg, J. P. 1973. In preparation.  
 Casse, J. L., and C. A. Muller. 1973. *Astron. Astrophys.* In press.  
 Chandrasekhar, S. 1950. *Radiative Transfer*. London: Oxford University Press, pp. 24-35.  
 Christiansen, N. N. 1953. *Nature* 171:831.  
 ———, and J. A. Högbom. 1969 *Radiotelescopes*. London: Cambridge University Press.  
 Clark, B. G. 1968. *IEEE Trans., Ap-16*, 143.  
 Cochran, W. T., J. W. Cooley, D. L. Favin, H. D. Helms, R. A. Kaenel, W. W. Lang, G. C.

- Maling, Jr., D. E. Nelson, C. M. Rader, and P. D. Welch. 1967. *Proc. IEEE* 55:1664.
- Cohen, M. H. 1958. *Proc. IRE* 46:172.
- . 1969. *Ann. Rev. Astron. Astrophys.* 7:619.
- , and D. B. Shaffer. 1971. *Astron. J.* 76:91.
- Conway, R. G., and P. P. Kronberg. 1969. *Monthly Notices Roy. Astron. Soc.* 142:11.
- Cooley, J. W., and J. W. Tukey. 1965. *Math. Computations* 19:297.
- Elgaroy, D., D. Morris, and B. Rowson. 1962. *Monthly Notices Roy. Astron. Soc.* 124:395.
- Erickson, W. C., and J. R. Fisher. 1973. In preparation.
- Fomalont, E. B. 1968. *Astrophys. J. Suppl.* 15:203.
- Hanbury Brown, R. 1968. *Ann. Rev. Astron. Astrophys.* 6:13.
- Hinder, R., and Ryle, M. 1971. *Monthly Notices Roy. Astron. Soc.* 154:229.
- Högbom, J. A. 1974. Submitted to *Astron. Astrophys.*, in press.
- Kraus, J. D. 1966. *Radio Astronomy*. New York: McGraw-Hill.
- MacPhie, R. H. 1966. *IEEE Trans.*, Ap-14, 369.
- McCready, L. L., J. L. Pawsey, and R. Payne-Scott. 1947. *Proc. Roy. Soc. A*-190:357.
- Mills, B. J., and A. G. Little. 1953. *Australian J. Phys.* 6:272.
- Moffet, A. T. 1968. *IEEE Trans.*, Ap-16, 172.
- Moran, J. M., B. M. Burke, A. H. Barrett, A. E. E. Rodgers, J. A. Ball, J. C. Carter, and D. D. Cudabeck. 1968. *Astrophys. J.* 152:L297.
- Morris, D., V. Radhakrishnan, and G. A. Seielstad. 1964. *Astrophys. J.* 139:551.
- Moseley, G. F., C. C. Brooks, and J. N. Douglas. 1970. *Astron. J.* 75:1015.
- Nielsen, K. L. 1964. *Methods in Numerical Analysis*. New York: Macmillan.
- Radhakrishnan, V., J. W. Brooks, W. M. Goss, J. D. Murray, and W. J. Schwarz. 1971. *Astrophys. J. Suppl.* 24:1.
- Read, R. B. 1963. *Astrophys. J.* 138:1.
- Rogstad, D. H., G. W. Rougoor, and J. B. Whiteoak. 1967. *Astrophys. J.* 150:9.
- Ryle, M. 1952. *Proc. Roy. Soc. A*-211:351.
- . 1960. *J. IEE* 6:14.
- . 1962. *Nature* 194:517.
- , and A. Hewish. 1960. *Monthly Notices Roy. Astron. Soc.* 120:220.
- , and D. D. Vonberg. 1946. *Nature* 158:339.
- Stanier, H. M. 1950. *Nature* 165:354.
- Swenson, G. W. 1969. *Ann. Rev. Astron. Astrophys.* 7:353.
- Wade, C. M. 1970. *Astrophys. J.* 162:381.
- Weiler, K. W. 1973. *Astron. Astrophys.* 26:403.
- Wild, J. P. 1967. *Proc. Inst. Radio Electron. Engrs. Australia* 28:279.